

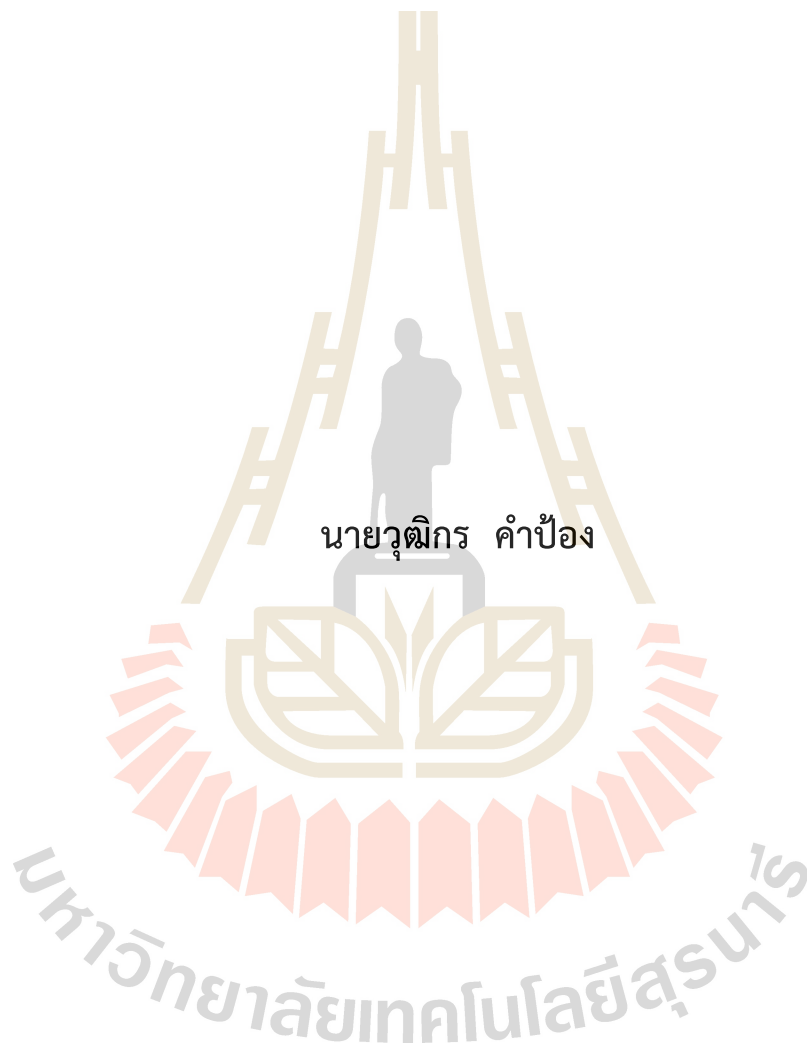
DEVELOPEMENT OF ALGORITHMS FOR OPTIMIZING FLOWS
CONTRAST IN OPTICAL COHERENCE TOMOGRAPHY ANGIOGRAPHY



WUTTIKORN KAMPONG

A Thesis Submitted in Partial Fulfillment of the Requirements for the
Degree of Master of Science in Physics
Suranaree University of Technology
Academic Year 2022

การพัฒนาอัลกอริทึมสำหรับเพิ่มความชัดในการถ่ายภาพหลุดเลื้อดด้วย
ออฟติคคอลโคเฮียเรนซ์โทโมกราฟี



นายวุฒิกร คำป้อม

วิทยานิพนธ์นี้เป็นส่วนหนึ่งของการศึกษาตามหลักสูตรปริญญาวิทยาศาสตรมหาบัณฑิต
สาขาวิชาฟิสิกส์
มหาวิทยาลัยเทคโนโลยีสุรนารี
ปีการศึกษา 2565

DEVELOPEMENT OF ALGORITHMS FOR OPTIMIZING FLOWS CONTRAST IN OPTICAL COHERENCE TOMOGRAPHY ANGIOGRAPHY

Suranaree University of Technology has approved this thesis submitted in partial fulfillment of the requirement for a Master's Degree.

Thesis Examining Committee



(Assoc. Prof. Dr. Puangratana Pairor)

Chairperson



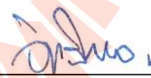
(Assoc. Prof. Dr. Panomsak Meemon)

Member (Thesis Advisor)



(Dr. Witwat Nuansing)

Member



(Dr. Ittipon Fongkaew)

Member



(Dr. Narong Chanlek)

Member



(Assoc. Prof. Dr. Yupaporn Ruksakulpiwat)

Vice Rector for Academic Affairs

and Quality Assurance



(Prof. Dr. Santi Maensiri)

Dean of Institute of Science

วุฒิกร คำป้อม : การพัฒนาอัลกอริทึมสำหรับเพิ่มความชัดในการถ่ายภาพหลอดเลือดด้วย
ออฟติกคอลลโคเฮียเรนซ์โทโมกราฟี (DEVELOPEMENT OF ALGORITHMS FOR
OPTIMIZING FLOWS CONTRAST IN OPTICAL COHERENCE TOMOGRAPHY
ANGIOGRAPHY) อาจารย์ที่ปรึกษา : รองศาสตราจารย์ ดร.พนมศักดิ์ มีมนต์, 46 หน้า

คำสำคัญ : โอซีที, การถ่ายภาพหลอดเลือด, แอมพลิฟิเคชันคอนทราสต์, ความแปรปรวนของ สเปกเคิล,
ความแปรปรวนของสเปกเคิลต่อค่าเฉลี่ย

ในการศึกษานี้ ระบบโอซีทีแองจิโอกราฟี (OCTA) ได้ถูกสร้างขึ้นเพื่อใช้งานร่วมกับระบบ
ถ่ายภาพออฟติกคอลลโคเฮียเรนซ์โทโมกราฟีในโดเมนสเปกตรัม (SD-OCT) ที่ใช้สเปกโตรมิเตอร์ใน
การตรวจจับสัญญาณ ซึ่งสร้างขึ้นโดยใช้หลักการแทรกสอดแสงแบบไมเคิลสัน โดยได้เลือกใช้เทคนิค
การวิเคราะห์สเปกเคิล 3 เทคนิค ได้แก่ เทคนิคการวัดแอมพลิฟิเคชันคอนทราสต์ (AD) เทคนิคการวัด
ความแปรปรวนของสเปกเคิล (SV) และเทคนิคการวัดความแปรปรวนของสเปกเคิลต่อค่าเฉลี่ย (SMV)
ซึ่งผู้วิจัยได้พัฒนาอัลกอริทึม SMV ขึ้นเองเพื่อเพิ่มประสิทธิภาพของระบบ OCTA ใน SD-OCT ให้มาก
ขึ้น นอกจากนี้ ยังได้ศึกษาเทคนิคเสริม 2 เทคนิค ได้แก่ เทคนิคการแยกสเปกตรัม (SS) และเทคนิค
การเฉลี่ยพิกเซล (pa) เพื่อเพิ่มประสิทธิภาพของระบบด้วยอีกทาง อีกทั้ง ในการเปรียบเทียบ
ประสิทธิภาพของอัลกอริทึมทั้งหมดที่สร้างขึ้น ผู้วิจัยได้สร้างแบบจำลองการไหลของเลือดใช้หลอด
คาปิลารีฝังไว้ในเจลของสารละลายยางนมเจือจาง เสมือนเป็นเส้นเลือดฝอยที่ฝังอยู่ใต้ผิวหนัง และเพื่อ
จำลองการไหลของเลือดภายในหลอดเลือดที่อยู่ใต้ผิวหนัง สารละลายยางนมเจือจางถูกปั๊มผ่านหลอด
คาปิลารีด้วยอัตราเร็ว 0.3 – 3.5 มิลลิเมตรต่อวินาที โดยใช้เข็มฉีดยากับมอเตอร์ที่ควบคุมโดย
คอมพิวเตอร์ ประสิทธิภาพของแต่ละอัลกอริทึมของโอซีทีแองจิโอแกรมถูกวัดจากค่าอัตราส่วนความชัด
สัมพัทธ์เมื่อเทียบกับสัญญาณรบกวน (rel-CNR) ซึ่งจากการวิเคราะห์และเปรียบเทียบพบว่า
อัลกอริทึม SMV ซึ่งเป็นอัลกอริทึมที่ผู้วิจัยพัฒนาขึ้นเอง สามารถให้ค่า rel-CNR สูงสุด และเมื่อนำ
อัลกอริทึม SMV ใช้ร่วมกับเทคนิคการแยกสเปกตรัมแล้ว พบว่าได้ค่าประสิทธิภาพของระบบที่ดีขึ้น
กว่าการใช้อัลกอริทึม SV ถึง 280%.

สาขาวิชาฟิสิกส์

ปีการศึกษา 2565

ลายมือชื่อนักศึกษา

ลายมือชื่ออาจารย์ที่ปรึกษา

WUTTIKORN KAMPONG : DEVELOPEMENT OF ALGORITHMS FOR OPTIMIZING
FLOWS CONTRAST IN OPTICAL COHERENCE TOMOGRAPHY ANGIOGRAPHY.
THESIS ADVISOR : ASSOC. PROF. PANOMSAK MEEMON, Ph.D. 47 PP.

Keyword : OCT, angiography, amplitude decorrelation, speckle variance, speckle-to-mean variance.


In this work, optical coherence tomography angiography (OCTA) was implemented on a spectrometer-based spectral domain OCT (SD-OCT) that was built on a Michelson interferometer. Three methods of speckle analysis were implemented, i.e., amplitude decorrelation (AD), speckle variance (SV), and speckle to mean variance (SMV). The SMV is an in-house developed algorithm designed to accommodate the poor signal-to-noise ratio performance of the spectrometer-based SD-OCT. Auxiliary methods such as split-spectrum (SS) and pixel averaging (PA) were used to increase the performance. To compare the performance of the implemented algorithms, a flow phantom was constructed by embedding a capillary tube inside a diluted milk gel that represented static tissue. To mimic blood flow beneath the skin, diluted milk was pumped through the capillary tube at speeds ranging from 0.3 to 3.5 mm·s⁻¹ using a syringe pump system. The performance of each OCTA algorithm, in terms of relative contrast-to-noise ratio (rel-CNR), was measured and compared. The results show that the SMV algorithm provided the highest rel-CNR. Then the split-spectrum method was applied with SMV to achieve the highest improvement over the performance of the SV algorithm of 280%.

School of Physics

Academic Year 2022

Student's Signature

Advisor's Signature



ACKNOWLEDGMENTS

I would like to express my sincere thanks to my thesis advisors, Assoc. Prof. Dr. Panomsak Meemon, for his invaluable help and constant encouragement throughout the course of this research. I am most grateful for his teaching and advice, not only on the research methodologies but also on many other methodologies in life. This thesis would not have been completed without all the support that I have always received from him.

In addition, I am grateful to Dr. Sorawis Sangtawesin, Dr. Wanvisa Talataisong, Jadsada Saetiew for his expert advice and research equipment support. I also thank DPST project, NRCT, and Suranaree University of Technology for the financial support. I am also grateful to committee for their valuable comments and suggestions.

Finally, I most gratefully acknowledge Wanna Wongsang, Kuljira Smithipon, Jiraporn Saenjae, and my friends for all their support throughout the period of this research.

Wuttikorn Kampong

มหาวิทยาลัยเทคโนโลยีสุรนารี

CONTENTS

	Page
ABSTRACT IN THAI.....	I
ABSTRACT IN ENGLISH.....	II
ACKNOWLEDGMENTS.....	III
CONTENTS.....	IV
LIST OF TABLES.....	VI
LIST OF FIGURES.....	VII
CHAPTER	
I INTRODUCTION.....	1
1.1 Research objectives.....	2
1.2 Research hypothesis.....	3
II LITERATURE REVIEWS.....	4
2.1 Optical coherence tomography (OCT)	4
2.2 OCT angiography algorithm.....	5
2.1.1 Intensity-based OCTA techniques.....	6
2.1.2 Phase-based OCTA techniques.....	9
2.1.3 Complex-based OCTA techniques.....	9
2.1.4 Split spectrum technique.....	9
III METHODS.....	12
3.1 Imaging system.....	12
3.2 OCTA algorithms.....	12
3.2.1 Main algorithms.....	12
3.2.2 Study the behavior of the main OCTA algorithms.....	13

CONTENTS (Continued)

		Page
	3.2.3 Auxiliary methods.....	17
	3.3 Experimental design.....	23
	3.4 Data analysis.....	24
	3.4.1 Algorithm's performance.....	24
	3.4.2 Algorithm verification.....	24
IV	RESULTS AND DISCUSSION.....	27
	4.1 Algorithm validation: vibration detection.....	27
	4.2 Differentiation of BMF and TMM detection.....	28
	4.3 Performance comparison.....	34
V	CONCLUSION.....	38
	REFERENCES.....	40
	CURRICULUM VITAE.....	46

LIST OF TABLES

Table	Page
1	SNR of the choriocapillaris imaging..... 6
2	Vascular SNR of 3 auxiliary angiography algorithms..... 7



LIST OF FIGURES

Figure	Page
1 Schematic of a Michelson interferometer.....	4
2 Color map of possible value of angiography range when intensity was set 1 – 255 and $N = 2$. (a) SV's possible value, and (b) AD's possible value.....	14
3 Noise-threshold diagram.....	14
4 Example of AD's value when noise-threshold is set to be 50.....	15
5 Simulated intensity for $n = 5000$ data-sets with randomized value that used in algorithms' range study.....	16
6 Angiography value calculated from the simulated intensity data-sets with no noise-threshold.....	16
7 Angiography value calculated from the simulated intensity data-sets that used SMV to calculate the variation of each simulated data-set.....	17
8 Gaussian curve.....	19
9 The superposition of all split-spectrum bands is flat-top Gaussian curve.....	21
10 Position of each narrower bands in term of the distance d and R	22
11 The flat-top superposition curve of all narrower bands with $fwhm = 0.6$ FWHM when vary M	22
12 The relationship between M and parameter c is linear.....	22
13 Raw OCT spectrum and 4 split spectra.....	22
14 The averaging technique uses 3×3 -pixel of OCT intensity.....	23
15 Schematic of angiography.....	24
16 Vibration of glass plate experimental setup.....	25
17 Flow phantom imaging experimental setup under the detector of OCT Imaging system.....	26
18 The data inside the yellow boxes represent samples of moving glass plate was used to be analyzed.....	27

LIST OF FIGURES (Continued)

Figure	Page
19	Comparison angiography value of static and vibrating glass plates, and top and bottom plate's surfaces..... 27
20	An OCT intensity image of flow phantom..... 29
21	Comparison of SV value in 3 regions at varied flow-speed, and example of pa-FS's threshold (dash line). If SV value is below the line, it will be classified to be static..... 30
22	Comparison of angiography value difference (flow – gel_2) in 3 regions at varied flow-speed 33
23	Image of a no-flow BMF inside a capillary at single lateral position (x)..... 34
24	Performance comparison in term of CNR..... 35
25	Performance comparison in term of rel-CNR..... 36
26	Performance comparison in term of rel-CNR..... 36
27	OCTA algorithm performance comparison..... 37



LIST OF ABBREVIATIONS

AD	Amplitude decorrelation
Av.	Average
BMF	Blood mimic fluids
CNR	Contrast to noise ratio
FS	Full spectrum
NC	Nailfold capillaroscopy
NVC	Nailfold videocapillaroscopy
OCT	Optical coherence tomography
OCTA	Optical coherence tomography angiography
Pixel av.	Pixel averaging
rel-CNR	Relative contrast to noise ratio
SD-OCT	Spectral domain OCT
SLE	Systemic lupus erythematosus
SMV	Speckle to mean variance
SS	Split spectrum
SSc	Systemic sclerosis

CHAPTER I

INTRODUCTION

In present, there are new gold standards of nailfold microvasculature imaging techniques such as nailfold capillaroscopy (NC) and nailfold videocapillaroscopy (NVC). However, their price is too high. Many specialists do not access these technologies. Nailfold videocapillaroscopy (NVC) is a straightforward tool utilized for diagnosing various abnormalities. It has shown positive results in patients with interstitial lung disease, connective tissue disease, rheumatoid arthritis, systemic sclerosis (SSc), hypersensitivity pneumonia, primary SjÖgren's syndrome, mixed connective tissue disease, systemic lupus erythematosus (SLE), and others (D. Sambataro et al., 2020). Therefore, NVC, or nailfold vascular imaging, holds significant potential in the modern era of clinical diagnosis and treatment.

The alternative instrument of dermatoscopy is widely used. Fortunately, this technology has capability to work as NC's function, but it has limitation of magnification. Its limitation of specifying the pattern change in early abnormality (de Carlo et al., 2015, Leitgeb et al., 2014, Sadda, 2017, Mahnaz Etehad Tavakol et al., 2015, Darryn Rennie, 2015).

The 21st century, people prefer a modern technology in every related life part. Especially, medical instruments are required to have lower prices which every hospital; and clinic able to access that technology. The more convenient and more safety technology is also essential. Many times, patients went to see a doctor to treat their health problem. It took a long time and did not complete at once. Both patients and doctors desire a new technique which takes a shorter time. Moreover, they are looking for a non-invasive technique for diagnosis and treatment patients. In addition, it will be an advanced benefit if many functions are combined in an instrument.

In this study, a new technology of nailfold microvasculature imaging will be discussed. Nailfold microvascular pattern can help in diagnosis of the possibility of connective tissue disease. It is also a tool for analysis microvascular abnormalities in autoimmune rheumatic diseases (Cutolo et al., 2006, Shahipasand et al., 2019). The microvascular damage in SSc pattern is related with the sclerodermic microangiopathy and the rheumatic disease, as well as ophthalmic disease (Cutolo et al., 2006, Shahipasand et al., 2019). It also provides advantages in other studies of lung disease, corona disease, and can be used as a monitor for drug effects (Yue Wang, 2019). To provide these benefits in this era, the old standard technique of nailfold microvasculature like fluorescein angiography (FA) and indocyanine green angiography (ICGA) (de Carlo et al., 2015, Leitgeb et al., 2014, Lihong V. Wang, 2007, Sadda, 2017) should be canceled.

It was reported that a commercial ophthalmic SD-OCT imaging system (S. Shahipasand et al., 2019) has potential to evaluate nailfold capillaroscopy, and a SD-OCT imaging system with a central wavelength of 1290 nm and a -3 dB bandwidth of 80 nm (Li-Bin Don et al., 2022) can image the nailfold angiography as well as quantify the capillary density and the capillary diameter. However, it quantifies capillary size larger than that provided by capillaroscopy technique.

As discussed above, there is a big opportunity for developing an OCTA imaging system in nailfold microvasculature. The OCTA might be cheaper and provide higher performance than the expensive standard technique of NC and NVC.

1.1 Research objectives

This thesis aims to:

- 1) Implement and verify OCTA algorithms on a spectral domain OCT imaging system.
- 2) Compare the OCTA algorithms' performance in experiments of flow phantom imaging.

1.2 Research hypothesis

- 1) The OCTA algorithm can be implemented on an available custom-built spectral domain OCT imaging system.
- 2) Imaging a reflecting surface will perform as an image including intensity at only the surface position and no or low intensity at other position. When the reflecting surface is vibrated, the position of the intensity is vibrated. That is demonstration of intensity changing when repeat scan the surface at the same position with varied time. If the implemented OCTA algorithm detected the variation of OCT signal, then the algorithm can detect the vibrated reflected surface.
- 3) The blood flow inside capillary is approximately 0.3 – 1.0 mm/s in capillary. The diluted milk solution with appropriate concentration was driven to flow inside a vessel that mimics blood fluids flow in capillary. The flow speed can be calculated by using a continuous equation controlling the flow rate of the fluids driven out of a syringe. If the implemented OCTA imaging system can differentiate blood flow from static tissue in nailfold, then the OCTA imaging system differentiates flow from static tissue in flow phantom.
- 4) Speckle variance (SV), amplitude decorrelation (AD), and speckle-to-mean variance (SMV) can provide enough performance for nailfold microvasculature imaging. One of them provides the highest performance.
- 5) The auxiliary method including split-spectrum (SS) and pixel-averaging (pa) methods will increase the main algorithm's performance.

CHAPTER II

LITERATURE REVIEWS

2.1 Optical coherence tomography (OCT)

Optical coherence tomography (OCT) technique, which was invented in early 1990s, is an optical imaging technique that can provide high-resolution images, and capability of monitoring 3D image in instantaneous time (L. V. Wang and Wu, 2012). OCT is a non-invasive technique, which causes no harm to biological tissue or any sample. It is based on low coherence light interferometer, such as Michelson interferometer.

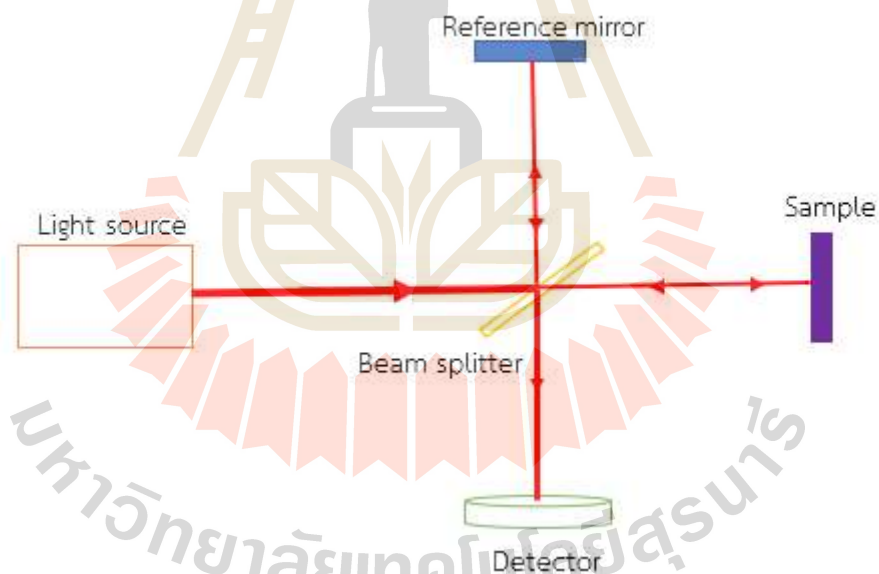


Figure 1 Schematic of a Michelson interferometer.

Basically, laser light from a source will be split into two beams. One of them propagates in the reference arm, and another beam propagates in the sample arm of an OCT system as shown in Figure 1. The reflection and backscattering light will be recombined and become the spectral interference or OCT signal. The interferogram

data is detected by a detector, which is a digital line-scan camera of spectrometer for SD-OCT system. The spectral interferogram or OCT signal $S(\lambda)$ is given by:

$$S(\lambda) = |E_R(\lambda) + E_S(\lambda)|^2 = |E_R(\lambda)|^2 + |E_S(\lambda)|^2 + 2\text{Re}\{E_R(\lambda) * E_S(\lambda)\} \quad (1)$$

where $E_R(\lambda)$ and $E_S(\lambda)$ are back-reflection and backscattering field of the electromagnetic wave from reference mirror and from the sample arm, respectively. λ is wavelength of laser light. The magnitude of these signal depends on λ and includes delay and attenuation.

The intensity from sample arm is usually much less than the intensity from reference arm, so the intensity of the second term can be ignored. Additionally, the pure information of interference of sample and reference will be obtained after vanishing the background intensity of reference. The pure interferometric signal $S_{\text{int}}(\lambda)$ is:

$$S_{\text{int}}(\lambda) = 2\text{Re}\{E_R(\lambda) * E_S(\lambda)\} \quad (2)$$

Before the pure signal can provide the depth information, we must map the parameter λ with $k = \frac{1}{\lambda}$ where k is wavenumber related with frequency of light. Now the signal is in term of $S_{\text{int}}(k)$. The next step is the process of discrete Fourier transform (DFT). DFT reconstructs the axial signal as function of axial position $S_{\text{int}}(z)$. The algorithm of DFT that widely used is Fast Fourier Transform (FFT). Scaling with logarithm function and normalization of the signal is the extra process after the FFT. That is the structural image of the living tissue or sample being already generated.

There are 2 types of OCT that are Time-domain OCT (TD-OCT) and Fourier-domain OCT (FD-OCT). FD-OCT can be Swept-source OCT (SS-OCT) or Spectral domain OCT (SD-OCT). The SS-OCT is the system, in which the light source can sweep the frequency of light. On the other hand, the SD-OCT is the system having a spectrometer as the detector.

2.2 OCT angiography algorithm

In the area of blood vessel, the moving erythrocyte, such as red blood cell,

causes the Doppler effect in OCT signal (Winkelmann et al., 2019). The frequency or phase of the signal is shifted. Normal structural OCT image cannot be used to generate the vasculature images. To solve this problem, one needs to analyze the doppler phase shift or the decorrelation of the amplitude signal. Doppler OCT is one of techniques that can quantify velocity of blood flow as well as generate angiogram (Ang et al., 2018, Chen and Wang, 2017, Carlo et al., 2015, Jia et al., 2012, Leitgeb et al., 2014, Spaide et al., 2018).

There are other techniques of motion contrast imaging that is OCTA technique, which is developed to improve and overcome limitations of the Doppler OCT. The hardware system of OCTA is similar to that of general OCT hardware. The differences are the methods of collecting data or data acquisition, and the decorrelation measurement is added into the processing of images. OCTA has been implemented in both SS-OCT and SD-OCT systems. Various OCTA techniques are developed to either only or both of generating the map of angiography and color map of flow speed. In term of information used for calculation, techniques of OCTA can be classified into three categories: intensity-based OCTA techniques, phase-based OCTA techniques, and complex-based OCTA techniques (C.-L. Chen and Wang, 2017). Most of all OCTA techniques do not depend on the angle enclosed with the propagation direction of the laser light.

2.1.1 Intensity-based OCTA techniques

Amplitude or intensity based OCTA algorithms include speckle variance (SV) (Mariampillai et al., 2008), correlation mapping (CM) (Jonathan et al., 2011), and split-spectrum amplitude decorrelation angiography (SSADA) (Jia et al., 2012). These algorithms use variance, decorrelation, cross-correlation, or absolute difference of OCT signal intensity between consecutive B-scans to map the microvasculature (Chen and Wang, 2017).

1) Speckle variance (SV)

SV is a method to measure the time-varying speckles due to movement of particle. Goodman found that the temporal speckle fluctuations at a point depends on the mean velocity of the scatterings (Chen and Wang, 2017). The speckle variance

concept is applicable to both the SD-OCT and SS-OCT systems. The SV signal can be obtained by scanning the same location any multiple N times, N used to be 4 in the first study and equal 3 in Mariampillai's study (Chen and Wang, 2017, Mahmud et al., 2013). The interframe SV can be computed as the following equation:

$$SV(z, x) = \frac{1}{N} \sum_{i=1}^N \left(I_i(z, x) - \bar{I}(z, x) \right)^2, \quad (3)$$

where \bar{I} is the average of intensity considering from N consecutive scans of the same set of pixels. Mariampillai et al. used a polygon-based SS-OCT system with a sweeping wavelength range of 112 nm centered at 1310 nm to image a flow phantom. The smallest vessels detectable by SV methods were 25 micron in diameter, and the axial resolution of 8 micron in tissue (Mahmud et al., 2013).

SV method provides high sensitivity, and independent of Doppler angle. It uses lower data storage compared with PV methods. Another key advantage is that it does not suffer from phase artifacts, thus complex methods of phase correction does not need (Jia et al., 2012). However, it also suffers from multiple scattering induced artifacts of the beneath the blood and interframe bulk tissue motion (Mahmud et al., 2013, Mariampillai et al., 2008).

2) Split-spectrum amplitude-decorrelation angiography (SS-AD)

SS-AD is proposed in 2012 by Jia et al. (Jia et al., 2012). It is an algorithm for calculate the decorrelation of the intensity with SS-OCT system. The idea of this methods is to improve SNR by degrading the axial resolution, which is always better than lateral resolution to be the same value of lateral resolution. The reduction can improve SNR without increasing the scan acquisition time. The methods of reducing sensitivity to noise in axial direction is by forcing the bandwidth to be narrower using bandpass filter. Normally, the Gaussian distribution is used to be the band filter. The bandpass method selects just a narrow range of frequency of full spectrum bandwidth. The frequency outside the window is mostly vanished. Moreover, multiple ranges of frequency are filtered. The new narrower bands provide the lower axial resolution (Δz) as the relation:

$$\Delta z = \frac{2 \ln 2}{\pi} \frac{\lambda_0^2}{\Delta \lambda}, \quad (4)$$

where $\Delta\lambda$ is the full width half maximum (FWHM) of the spectrum band, and λ_0 is the center wavelength.

To use entire ranges of the original spectrum information, the combination of all split bands (narrower bands) will be recombined together in the final step as the calculation equation below:

$$\text{SSAD}(z, x) = 1 - \frac{1}{N-1} \frac{1}{M} \sum_{i=1}^{N-1} \sum_{j=1}^M \left(\frac{I_{ij}(z, x) I_{(i+1)j}(z, x)}{\frac{1}{2} (I_{ij}^2(z, x) + I_{(i+1)j}^2(z, x))} \right), \quad (5)$$

where M is the number of split-spectrum, N is the number of consecutive B-scans at the same location, I_{ij} is the intensity in i -th B-scans of j -th split-spectrum at lateral location x and depth position z .

In the first implement of SS-AD, Jia et al. used $M=4$, $N=8$ (Jia et al., 2012). In 2015, Gao et al. (Gao et al., 2015) used the SS-AD algorithm on SD-OCT system by adjusting bandwidth of each split to maximize the flow phantom decorrelation SNR, and they found that $M=11$ of a flow phantom can maximize the decorrelation SNR or DSNR. In addition, this algorithm has limitations of the projection of other flow and still sensitive to noise from bulk motion (Jia et al., 2012).

3) Additional intensity-based OCTA technique

The SS-AD techniques combined and developed from split spectrum or bandpass filter technique and amplitude-decorrelation technique. In the other word, AD is the original of SS-AD or special condition of SS-AD with $M=1$. It can be called full-spectrum amplitude-decorrelation angiography (FS-AD) or amplitude-decorrelation angiography (AD) (Ang et al., 2018). It measures the decorrelation of the intensity signal as the equation below:

$$\text{AD}(z, x) = 1 - \frac{1}{N-1} \sum_{i=1}^{N-1} \left(\frac{I_{ij}(z, x) I_{(i+1)j}(z, x)}{\frac{1}{2} (I_{ij}^2(z, x) + I_{(i+1)j}^2(z, x))} \right). \quad (6)$$

Not only split-spectrum method was applied with AD or others algorithm, but pixel-averaging was also used for an auxiliary method that applied with the main methods. This method is often used to improve the qualities of the images.

2.1.2 Phase-based OCTA techniques

Phase based OCTA algorithms, beside phase-based doppler variance, is phase variance (PV) technique (Fingler et al., 2007), split-spectrum phase-gradient (SS-PGA) OCTA (Liu et al., 2016). Most of them provide the high axial resolution, especially phase-based OCTA (Chen and Wang, 2017). However, there are very sensitive to dominate bulk motion noise and artifact (Chen and Wang, 2017, Carlo et al., 2015, Jia et al., 2012, Spaide et al., 2018). For this reason, the algorithms of phase and complex OCTA require the removal of motion artifact.

2.1.3 Complex-based OCTA techniques

There is a group of complex-signal-based OCTA. This group includes optical microangiography (OMAG) (Wang, 2010, Wang et al., 2007), eigen-decomposition-based OMAG (S. Yousefi et al., 2011), imaginary part-based correlation mapping OCTA (Chen et al., 2015), SS-PGA and split-spectrum amplitude and phase-gradient angiography (SSAPGA). In addition, Imaginary part-based CMOCTA is proposed to solve blurry side effect due to increased correlation window size in CMOCTA. Since it includes both intensity and phase, it is able to detect the phase changes caused by red blood cell, which does not effect on the intensity (C. Chen and Wang, 2017, C. Chen et al., 2015). This method is more sensitive to tissue bulk motion and can provide images with higher sensitivity than provided from CMOCTA.

2.1.4 Split spectrum technique

The OCTA algorithms usually consist of the main technique and auxiliary techniques. One of the best available OCTA algorithms is SSADA algorithm proposed by Jia et al. in 2012. SSADA is an inter-frame mode of amplitude-based technique, consists of decorrelation technique and split-spectrum technique for the main and auxiliary technique, respectively. It is an intensity-based technique. This algorithm has been modified and implemented in SS-OCT for visualizing angiograph of optic nerve head and macular. After background subtraction and autocorrelation procedures, the full band spectrum of OCT information was split into several narrower bands. For each narrower band, the consecutive B-scans of the same location were then used to calculate the decorrelation. However, the entire bands recombined to utilize all the

speckle information in full spectrum (C. Chen and Wang, 2017, Gao, Liu, Huang, and Jia, 2015, Jia et al., 2012). Even though it has capability of providing very high signal to noise ratio (SNR) angiographic image, it must trade axial resolution and still has limitation of motion artifact.

The performance provided by no split spectrum techniques, e.g. SV, PV, and ADA, and split spectrum techniques, e.g. SSSV, SSPV, SSADA, were compared by Gorczynska et al. in 2015. The PV method provided higher SNR than SV and ADA algorithms, and applications of split spectrum technique tends to increase the SNR for each of the methods as shown in Table 1.

Table 1 SNR of the choriocapillaris imaging (Gorczynska, Migacz, Zawadzki, Capps, and Werner, 2016).

OCTA algorithm	SNR
SV	0.77 ± 0.04
SSSV	0.88 ± 0.04
ADA	1.01 ± 0.04
SSADA	1.05 ± 0.04
PV	1.34 ± 0.04
SSPV	1.38 ± 0.05

That is in the case of $M = 5$ and $N = 5$. Considering the difference of SNR, it is smaller than the error for SSADA-ADA and SSPV-PV. It was found that only split spectrum applied with SV has improved.

However, it was reported by Jia et al. that retina and choroidal angiography provided by SSADA method can improve SNR by 105% compared with the images provided by ADA (Chen and Wang, 2017, Gao et al., 2015, Jia et al., 2012). It can also provide higher performance compared with pixel-averaging method as shown in Table 2.

Table 2 Vascular SNR of 3 auxiliary angiography algorithms (Jia et al., 2012).

Auxiliary technique	SNR	Improvement of SNR
full spectrum	3.3 ± 0.8	N/A
average spectrum	5 ± 1	38.5%
split spectrum	6.8 ± 0.8	105 %

Gao et al. optimized SSADA on SD-OCT system. It was found that, for 2 consecutive B-scans, the maximum SNR depends on number of spectral split (M). For angiography of flow phantom, the highest SNR was achieved when $M=11$; and if M increases, it found no significance of improvement (Gao et al., 2015).

Therefore, the auxiliary technique of split spectrum has capability of improvement the SNR of OCTA images when the M and N is optimized. In addition, SSSV seem to have potential of providing higher performance compared with SSADA. However, it must be an answer of specific application that we need to find.



CHAPTER III

METHODS

3.1 Imaging system

In my work, an OCT imaging system of our custom-developed OCT imaging systems was used to collect experimental data which is then used in angiography value calculation. The imaging system is a spectral-domain OCT that was constructed on Michelson interferometer. The imaging system operated by using low-coherence NIR light with center wavelength of 835 nm and bandwidth (FWHM) of 120 nm. The detector of the system is an in-house-invented spectrometer. It includes line-scan camera of 2048 pixels with the scanning rate of 51 kHz. It is complementary metal-oxide-semiconductor (CMOS) (Mars2048-L51gm, CONTRASTECH) with a small pixel size of 10 mm x 10 mm.

3.2 OCTA algorithms

3.2.1 Main algorithms

This work aims to implement speckle variance (SV) and amplitude-decorrelation (AD) algorithms. The SV and AD equations are shown as equation (3) and (6) respectively.

It was reported that they have ability to segment flow out of the static tissue, give high performance of illustrate angiography images, and do not depend on the vessel orientation. Thus, SV and AD algorithms will be the main OCTA algorithms in this study.

3.2.2 Study the behavior of the main OCTA algorithms

To understand the behaviour of the algorithms that result the angiography value, there are 2 studies.

- 1) Generating a map of angiography range when using $N = 2$.
- 2) Generating random intensity set of $N = 8$ to calculate angiography value from the random intensity data sets.

1) The intensity domain was set to be 1 – 255 as 8-binary bit but no zero to prevent the problem of dividing by zero. It was found that the range of the possible value of SV and AD expressed as figure 2.

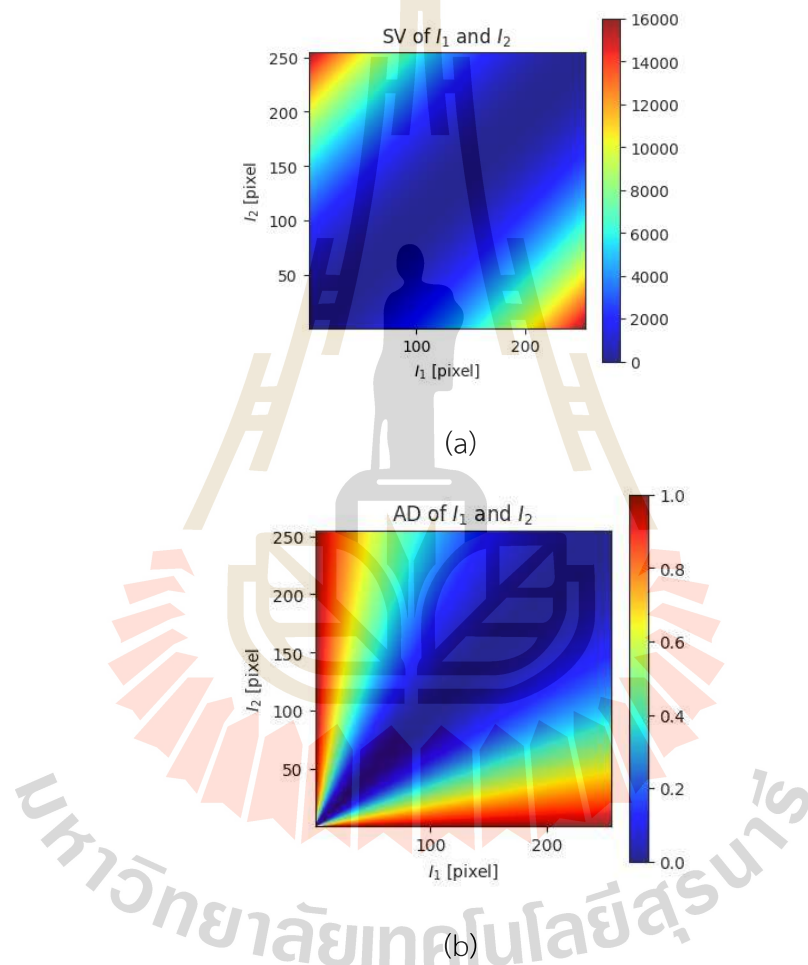


Figure 2 Color map of possible value of angiography range when intensity was set to be 1 – 255 and $N = 2$. (a) SV's possible value, and (b) AD's possible value.

As shown in the angiography value's map, the SV value was resulted in a wide range. The magnitude of SV value depends on the intensity strength. In the other hand, the AD value was resulted in limited range of 0 – 1. The high magnitude can be

obtained even through the intensity I_1 and I_2 are low strength. Meanwhile, the low intensity such as noise must be considered. Noise with low intensity can provide high magnitude of AD value that is unallowed. Thus, there is a method to prevent the problem. The noise-threshold should be set to vanish the false-variation with high magnitude of AD as figure 3.

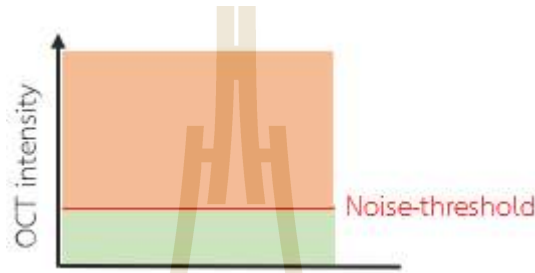


Figure 3 Noise-threshold diagram.

Then, the AD's value will be resulted narrower range and will result the maximum value of AD less than 1. For example, the noise threshold is set at intensity is equal to 50, then the AD's value will be lower than 0.7 as figure 4.

In this work the noise-threshold will be set by considering the averaging intensity of an OCT intensity image. The intensity which is lower than the threshold will be turn to equal to 1.

2) The algorithms were used to generate angiography value by using random number act as OCT image intensity. The OCT intensity was generated $n = 5000$ data-sets as 5000 position and each position was randomly generated 8 times for repetition to consider the variation at each position n as figure 5.

As seen in the figure 6a, the range of SV' value is unbounded. The maximum of SV value can be whatever positive number that depends on the strength of input-intensity. In the other hand, the range of AD's value is between 0 and 1. It's not easy to compare these two algorithms. Although the SV 's scale can be normalized by dividing SV' value by a constant number, there are no absolute maximum of SV 's

value. To obtain more reasonable comparison, I modified SV and obtain a new algorithm. That is speckle-to-mean variance (SMV) shown as equation (7):

$$\text{SMV}(z, x) = \frac{1}{N} \sum_{i=1}^N \left(\frac{I_i(z, x)}{\bar{I}(z, x)} - 1 \right)^2. \quad (7)$$

The SMV was also used to study its behaviour by using SMV that calculate the 8-randomized intensity of 5000 data-sets. The result as figure 7 shows that the range of SMV's value is between 0 and 1.5. Most of data-set is under 1, there are only 0.64% of data-set that are extremely various and provide SMV value higher than 1.

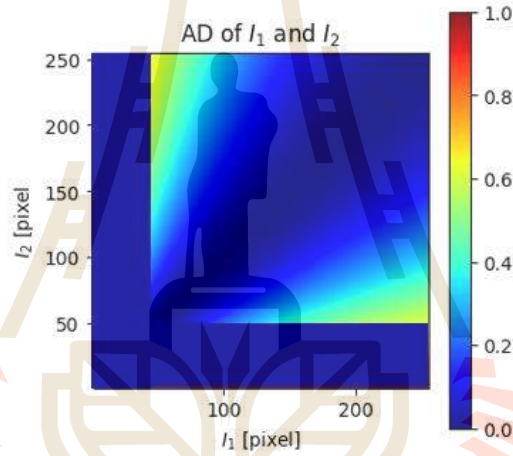


Figure 4 Example of AD's value when noise-threshold is set to be 50.

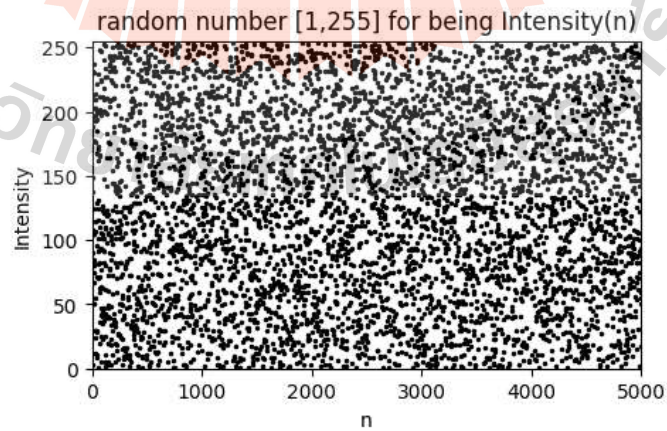


Figure 5 Simulated intensity for $n = 5000$ data-sets with randomized value that used in algorithms' range study.

On each position, 8-random numbers were calculated SV and AD values as shown in equation (1) and (2). The SV and AD algorithms result as figure 6.

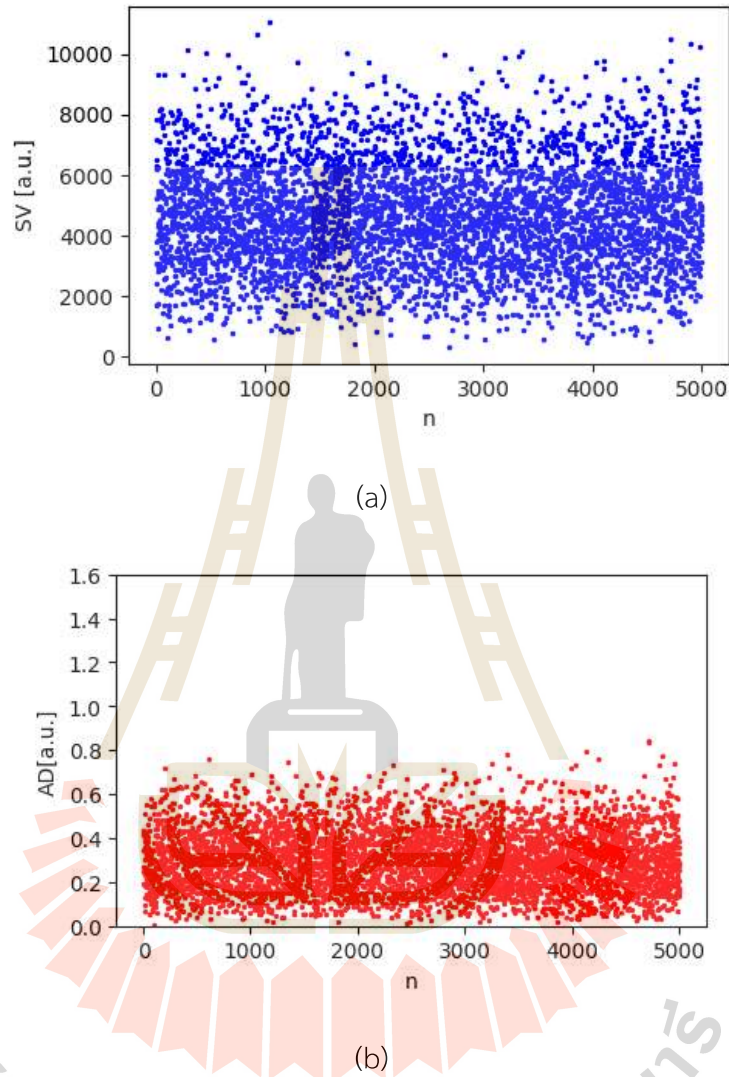


Figure 6 Angiography value calculated from the simulated intensity data-sets with no noise-threshold. Angiography value calculated by using OCTA algorithm: (a) SV, and (b) AD.

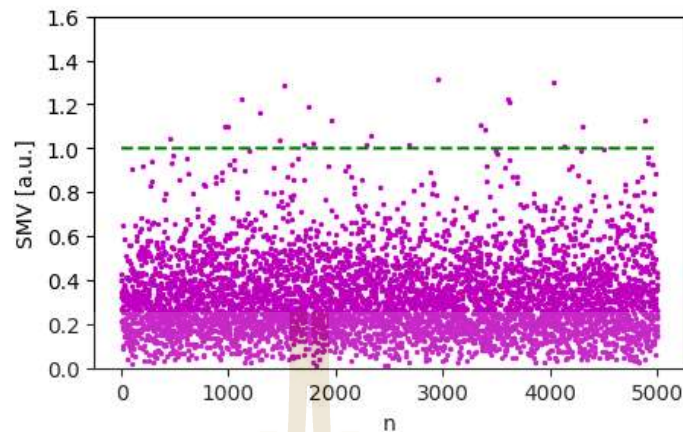


Figure 7 Angiography value calculated from the simulated intensity data-sets that used SMV to calculate the variation of each simulated data-set.

SMV does not take place SV as normalize scale of SV. However, The behavior of SMV is interesting. Fortunately, the SMV can be one in candidates. Moreover, to compare the OCTA algorithms has to use indirect comparison such as comparing in algorithms' performance.

3.2.3 Auxiliary methods

To improve the OCTA algorithms, there are one way to enhance the ability of each algorithm to provide higher performance. That is using auxiliary techniques such as split-spectrum technique, pixels-averaging technique. The auxiliary technique was usually used to improve SNR. In this work, the split-spectrum technique and pixel-averaging technique are also used to improve SNR for the aim of discovering the highest improvement OCTA algorithm.

1) The split-spectrum technique

Normally for an OCT image, the axial resolution is better than lateral resolution. When the image is constructed into 3-D information as well as resliced for top view

image, the apparent resolution is usually decided to equal to the worser or lateral resolution.

The split-spectrum method is a technique for filtering the original light spectrum band to become narrower. That means the new bandwidth (**fwbm**) is smaller than the original bandwidth (**FWHM**). The narrower bandwidth results in degrading the axial resolution. In the other hand, **fwbm** is also degrade the noise in spectrum that helps to improve the algorithm performance (**SNR**).

The split-spectrum technique is a technique that use gaussian curve to envelope the spectrum before taking the Fourier-transform. The gaussian filter has curve as figure 8 and the formular as

$$g(x) = \exp\left(-\frac{(x-r_m)^2}{2\sigma^2}\right), \quad (8)$$

where x is position in OCT signal spectrum, r_m is position of the m-th split-band center, and σ is standard deviation of the distribution curve $g(x)$.

Half maximum of $g(x)$ is 0.5, and full-width-half-maximum (**fwbm**) can be solved from $g(x)$ curve from:

$$g(x) = \frac{1}{2}. \quad (9)$$

From (4) and (5), we get

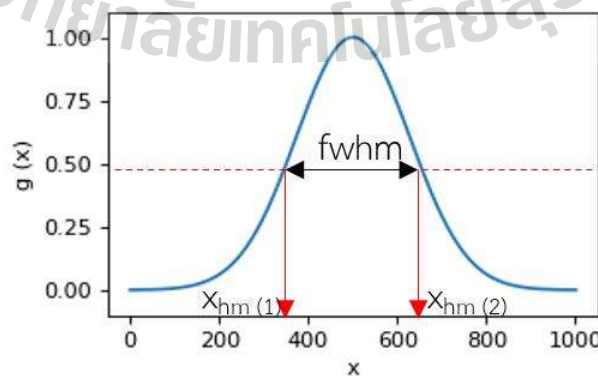


Figure 8 Gaussian curve.

$$x_{\text{hm}} = r_m \pm \sigma \sqrt{2 \ln 2} . \quad (10)$$

Therefore, the relation of **fwhm** and σ is

$$\text{fwhm} = 2\sigma \sqrt{2 \ln 2} \quad (11)$$

or $\text{fwhm} \approx 2.355\sigma ,$

and $\sigma = \frac{\text{fwhm}}{2\sqrt{2 \ln 2}} \quad (12)$

or $\sigma \approx \frac{\text{fwhm}}{2.355} .$

The $g(x)$ curve is designed by considering axial resolution (Δz) as equation (4). The narrower band should not be in resulting the Δz worser than the lateral resolution. In this study, the OCT imaging system use NIR light source of $\lambda_0 = 835 \text{ nm}$ and **FWHM** or $\Delta\lambda = 120 \text{ nm}$. The axial resolution is $2.6 \text{ }\mu\text{m}$ while the lateral resolution is $4.7 \text{ }\mu\text{m}$. That means the narrower bandwidth (**fwhm**) should provide axial resolution equal to $4.7 \text{ }\mu\text{m}$ for roughest. In other words, **fwhm** should be:

$$\text{FWHM} > \text{fwhm} > \frac{2.6}{4.7} \text{FWHM} .$$

In this study, **fwhm** was set to be 0.60 FWHM . Therefore, the calculated axial resolution of the image provided by this OCTA imaging system is $2.6/0.6 = 4.3 \text{ }\mu\text{m}$. The number of split-spectrum in this study is $M = 4$. The position of each split-spectrum band is defined by considering the superposition of all split-spectrum bands that should be a flat-top gaussian curve as figure 9. To obtain the split-spectrum bands as defined above, the relationship of curve's shape parameters was considered. The distance between two closest bands should be in terms of **fwhm**, and M as $d(\text{fwhm}, M)$. The position of each split-band center (R) that distance from the center position of the original OCT spectrum band (r_0) should be in term of **fwhm**, d , and M as $R_m(\text{fwhm}, M, d)$ and express the relationship between a gaussian filter curve and the other curve as figure 10. The superposition of all split-curves was simulated

as figure 11 when M was varied while fwhm was fixed. A parameter c helped to construct the formular of the relation express as:

$$d = \text{fwhm} \left(\frac{M}{c} \right). \quad (13)$$

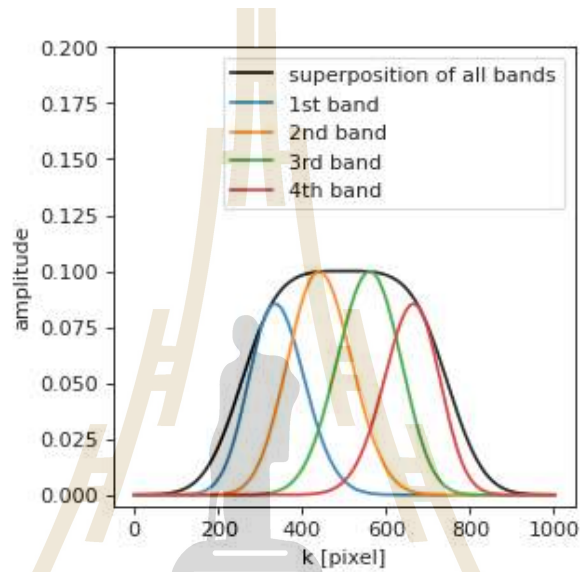


Figure 9 The superposition of all split-spectrum bands is flat-top Gaussian curve.

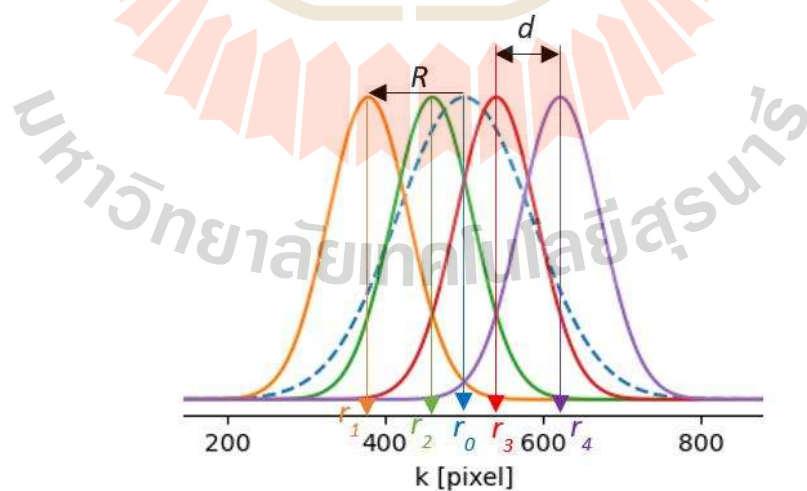


Figure 10 Position of each narrower bands in term of the distance d and R .

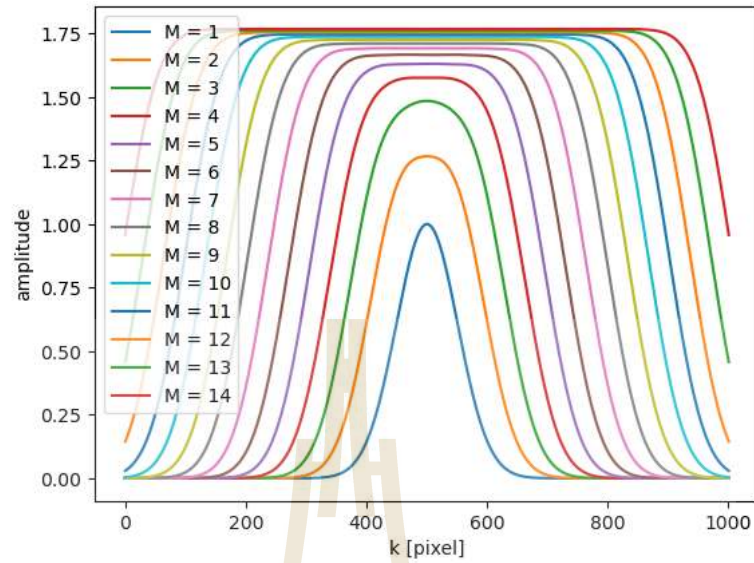


Figure 11 The flat-top superposition curve of all narrower bands with $\text{fwhm} = 0.6 \text{ FWHM}$ when vary M .

It was found that the parameter c value is vary when M was changed as figure 12, and the relationship between c and M is linear express as:

$$c = \sqrt{3M} - 1. \quad (14)$$

Therefore, the equation (16) is turned to be

$$d = \frac{\text{fwhm}}{\sqrt{3} - 1/M}. \quad (15)$$

When these Gaussian filters were used to apply with OCT spectrum and obtain the split-spectrum bands with narrower fwhm as figure 13.

2) Pixel-averaging methods

Sometime the speckle can be results in high variation, pixel averaging method is one technique that can help to decrease the high variation of the speckle. In this study, the averaging method will use 3x3-pixel of OCT intensity, then average to become intensity of the center pixel as shown in figure 14 and equation (16):

$$I(i, j) = \frac{1}{3} \cdot \frac{1}{3} \sum_{u=i-1}^{u=i+1} \sum_{v=j-1}^{v=j+1} I(u, v). \quad (16)$$

The averaged intensity images of each OCT images were then used to calculate the angiography value by candidate algorithms.

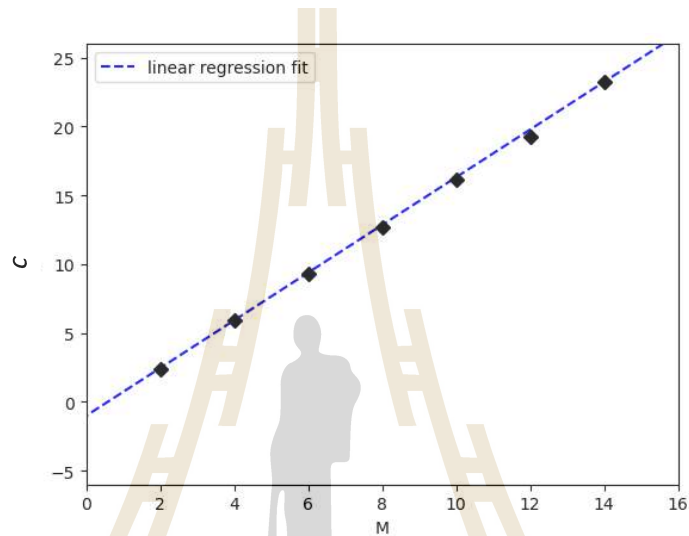


Figure 12 The relationship between M and parameter c is linear. It was fit by using linear regression and found that slope = $1.723 \approx \sqrt{3}$, y-intercept ≈ -1 , and coefficient of determination = 0.9999753.

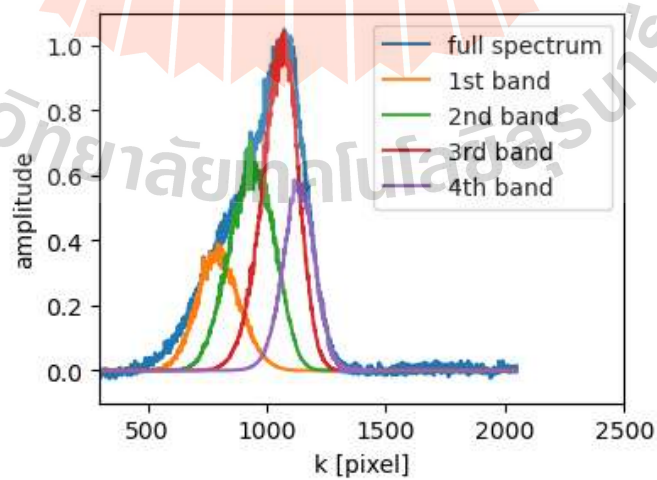


Figure 13 Raw OCT spectrum and 4 split spectra.

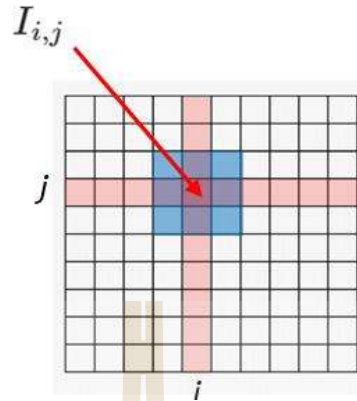


Figure 14 The averaging technique uses 3x3-pixel of OCT intensity.

In this study both split-spectrum method and pixel-averaging method are used for the aim to improve and compared the algorithm performance.

3.3 Experimental design

OCTA imaging was implemented on a spectrometer-based SD-OCT that was built on Michelson interferometer as shown in figure 15. First, the interference of the back-scattering $ES(\lambda)$ from a sample and the back-reflection light $ER(\lambda)$ from a reference mirror was captured by a custom-built high-speed spectrometer. Second, the acquired interference was subtracted by self-interference light for DC removal to obtain pure information $AC(\lambda)$. Third, the linear-in-wavelength spectral interference was interpolated to a linear-in-wavenumber signal $AC(k)$. Forth, the interpolated spectrum was Fourier transformed to obtain the depth information $I(z)$. Fifth, about 1000 depth-scans were acquired over a range of lateral position (x) to form an OCT speckle image $I(z, x)$. Finally, to generate angiography, image acquisition at the same location was repeated ($N = 8$), with the interframe time (dt) of 120 ms. The OCTA can differentiate blood vessel from static tissues by analyzing the variation of OCT speckle caused by moving erythrocyte in blood vessel.

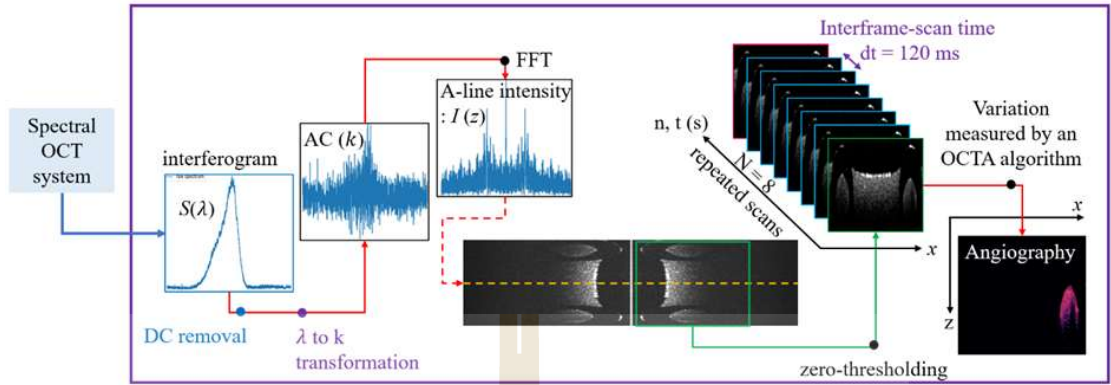


Figure 15 schematic of angiography measurement (reproduced and modified from W. Kampong et al. 2023).

3.4 Data analysis

3.4.1 Algorithm's performance

To compare the performance of the implemented algorithms, a flow phantom was built and used as a sample. The value of contrast to noise ratio (CNR) was defined and used as a parameter to compare the performance of the algorithms. The CNR was calculated as:

$$\text{CNR} = \frac{\bar{D}_{\text{flow}} - \bar{D}_{\text{static}}}{\sigma_{\text{static}}} \quad (17)$$

Where \bar{D} is angiography value provided by each algorithm, σ is standard deviation of the angiography value.

3.4.2 Algorithm verification

1) Algorithms validation using a vibrating reflector

To optimize the OCTA imaging system on our existing OCT system, the ability to differentiate the speckle fluctuation of each angiography algorithm was verified. An experiment was conducted to determine whether the algorithms were capable of measuring variation in the OCT signal or not. The extreme variation test was applied by using vibrating cover-slide glass as shown in figure 16. The glass plate was forced to

vibrate as sinusoidal wave with 4 Hz frequency by using a Piezo-vibrator device. We expected that, the vibrating glass plate should provide strong speckle variance while the static glass plate should provide less speckle variance. The represented data were analyzed and compared.



Figure 16 Vibration of glass plate experimental setup.

2) Detection of differentiate of BMF and TMM: flow phantom experiment

The performance of the algorithms was studied by imaging a flow phantom. The flow phantom was constructed by embedding a capillary tube of 0.5 mm inner diameter inside tissue mimic material (TMM) as shown in figure 16. The TMM was a bulk of gel composed of blood mimic fluids and gelatin. To mimic a blood flow beneath skin; dilute milk, mixed of 5% liquid milk and 95% water, was pumped through the right capillary tube with average flow speed of 0.3 to $3.5 \text{ mm}\cdot\text{s}^{-1}$ by using a syringe pump system. The left tube was filled with TMM (gel). The capillary tubes were embedded in TMM (gel). The represented data were analyzed and compared.

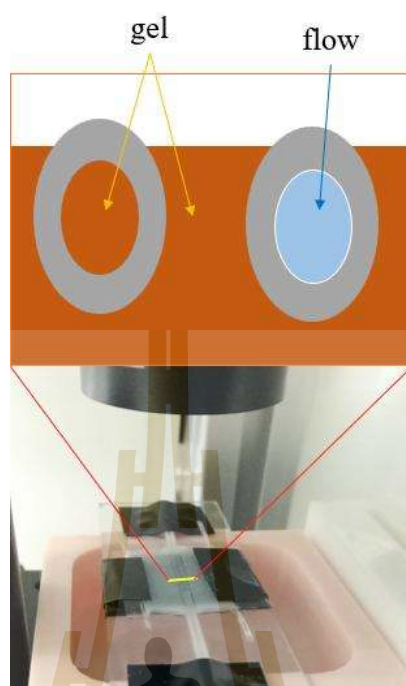


Figure 17 Flow phantom imaging experimental setup under the detector of OCT imaging system.

CHAPTER IV

RESULTS AND DISCUSSION

4.1 Algorithm validation: vibration detection

A glass plate was vibrated with 4 Hz that lower than the OCT's camera scan rate of 8.3 Hz. That allow the moving glass plate to be record the different axial position of the plate's surface. Thus, the speckle images of $N = 8$ images are expected to be varied. In analysis, the intensity of pixels inside the box in figure 18 was used as sample and analyzed by candidate OCTA algorithms. The results can be shown as figure 19.

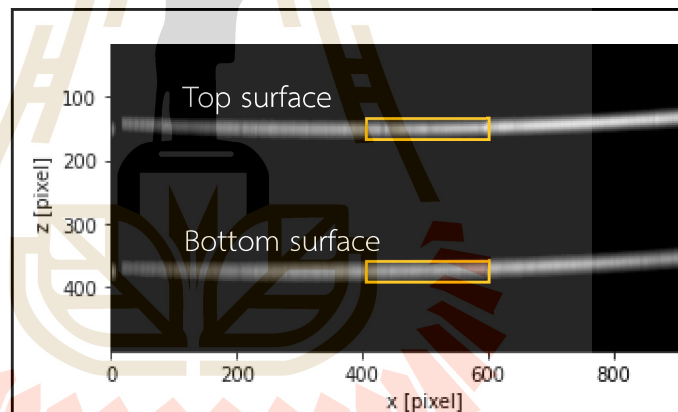


Figure 18 The data inside the yellow boxes represent samples of moving glass plate was used to be analyzed.

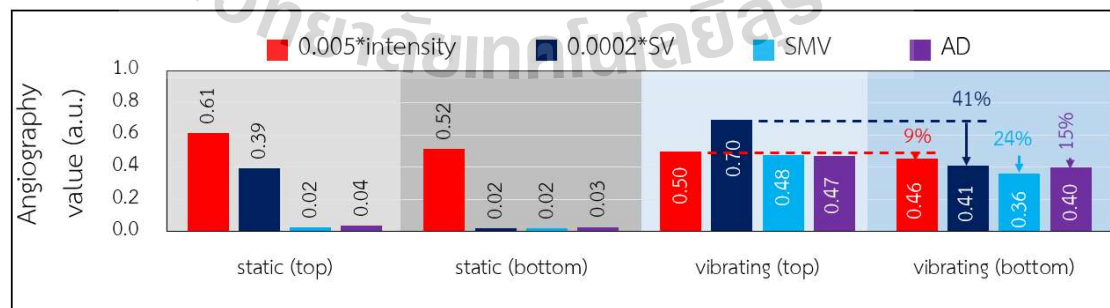


Figure 19 Comparison angiography value of static and vibrating glass plates, and top and bottom plate's surfaces (reproduced from W Kampong et al., 2023).

Figure 19 shows that the angiography value of the top and bottom surfaces of the vibrated cover-slide glass plate is approximately 10 times than that of the static surfaces. It confirms that the algorithms operated with our OCT system can differentiate the variation. It also shows that the intensity was only slightly dropped when the reflector was vibrated. In contrary, the strong changes were observed on all angiography algorithms. In addition, the angiography values of the bottom surface of the vibrated glass are smaller than that of the top surface. It implies that the angiography performance may depend on the intensity values of the OCT image. That might cause a problem of inequality of intensity when comparing an angiography value of two or more regions which have different intensity.

4.2 Differentiation of BMF and TMM detection

Data in highlight boxes in figure 20(a) representing no-flow (gel-1) in a vessel, static tissue (gel-2) outside a vessel, and flow of BMF (flow) inside a vessel were analyzed. First, the OCT intensity of all regions were compared. The figure 20(b) shows the averages of intensity (av intensity) in the highlight boxes of gel-1, gel-2, and flow. The results show that the OCT intensities of gel-2 or tissue which is outside vessel are higher than that of both flow and no-flow inside vessels for all experiments of varied flow-speed. Whereas av intensities of gel-1 or no-flow are lower than that of flow. That shows the intensity of 3 regions are not equal as expectation, however that provide a benefit of validation of flow's effect.

The variation of 8-repeated scans was analyzed. As figure 21, flow region of every flow speed experiment provided SV value higher than both that of gel-1 and gel-2 although gel-2's intensity is higher than flow's intensity. For more convenience, flow angiography value at each flow speeds of all algorithms were subtracted by that of gel-2 and resulted as figure 22. Since the angiography of gel-2 was higher than that of gel-1 for every algorithm and every flow speed. This confirms that the variation

effected from flow that dominates the SV value and overcomes the problem of inequality of intensity.

Figure 22 shows that flow was different and higher than static tissue. However, high flow speed was not much different than no-flow speed (0 mm/s). It implies that static tissue (gel) and no-flow fluids have different behavior.

For further investigation, a m-mode scan was analysis. The detector pointed at single lateral position along the interval of recording spectrum and then was analyzed and resulted as figure 23. The structural image or intensity image shows that no-flow fluids are not absolutely resting. If particle is resting along the time, the image will show a continuous solid line along the time. There are a lot of discontinuous lines in the image. That means no-flow includes slow moving scatterers in the capillary. This phenomenon might be effect of Brownian motion.

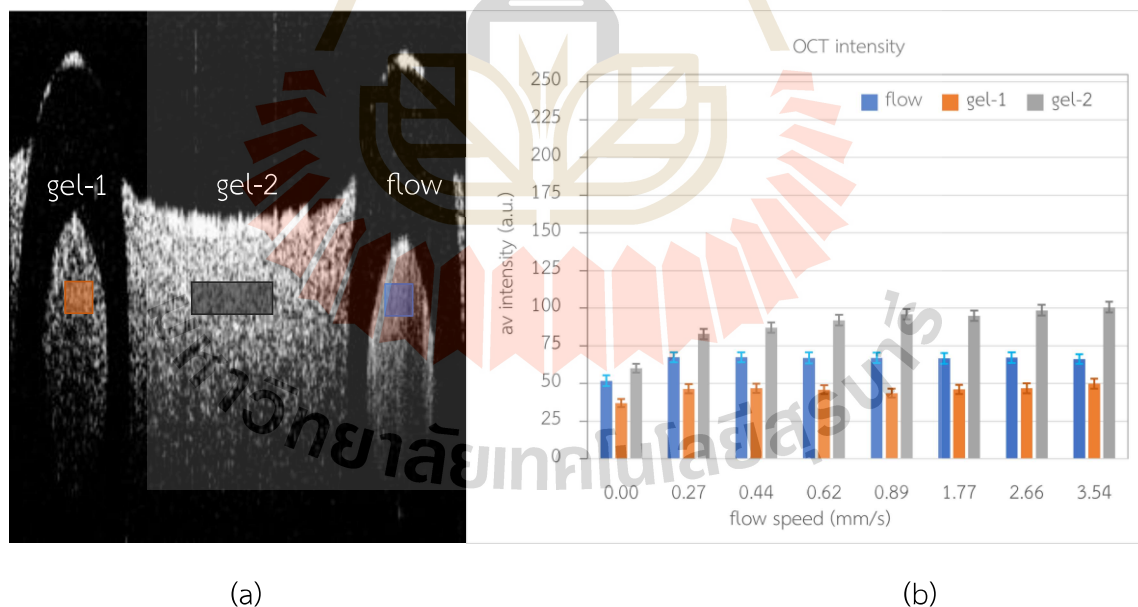


Figure 20 An OCT intensity image of flow phantom. (a) show the regions of no-flow, static tissue, and flow, (b) comparison of av intensity value in 3 regions at varied flow-speed.

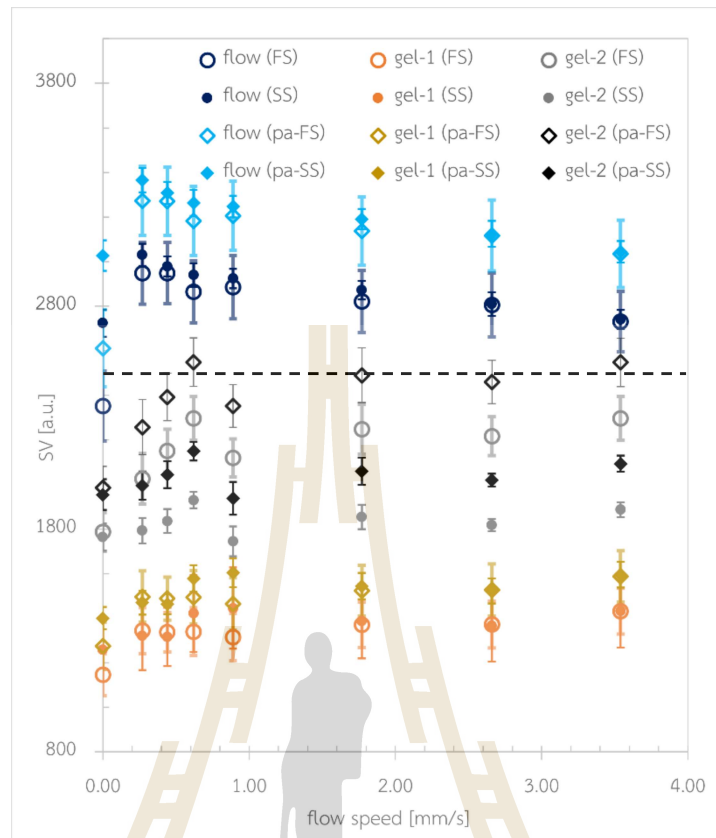


Figure 21 Comparison of SV value in 3 regions at varied flow-speed, and example of pa-FS's threshold (dash line). If SV value is below the line, it will be classified to be static.

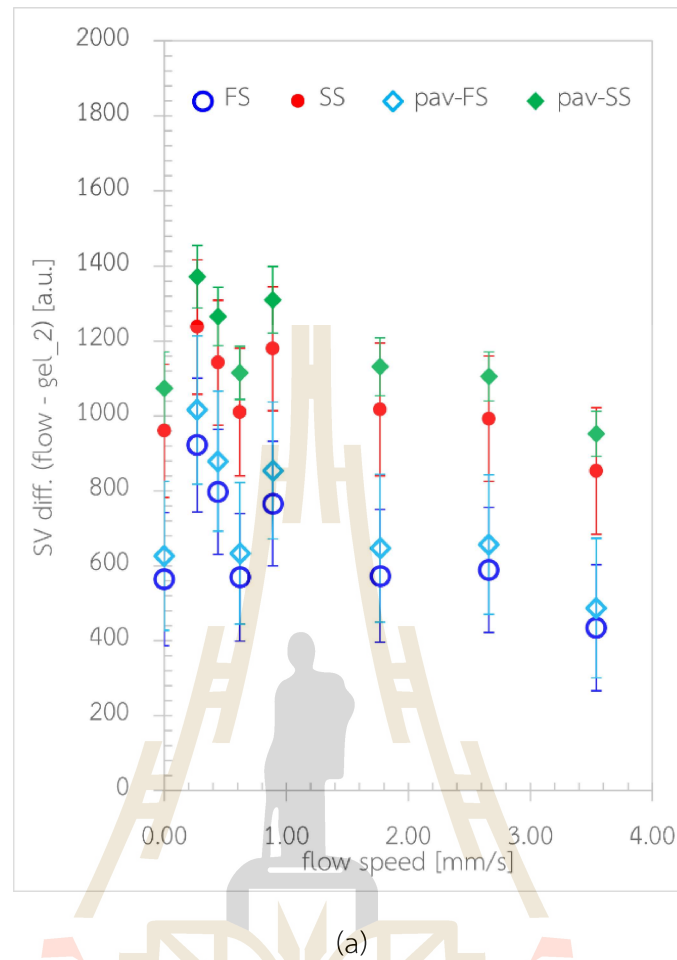
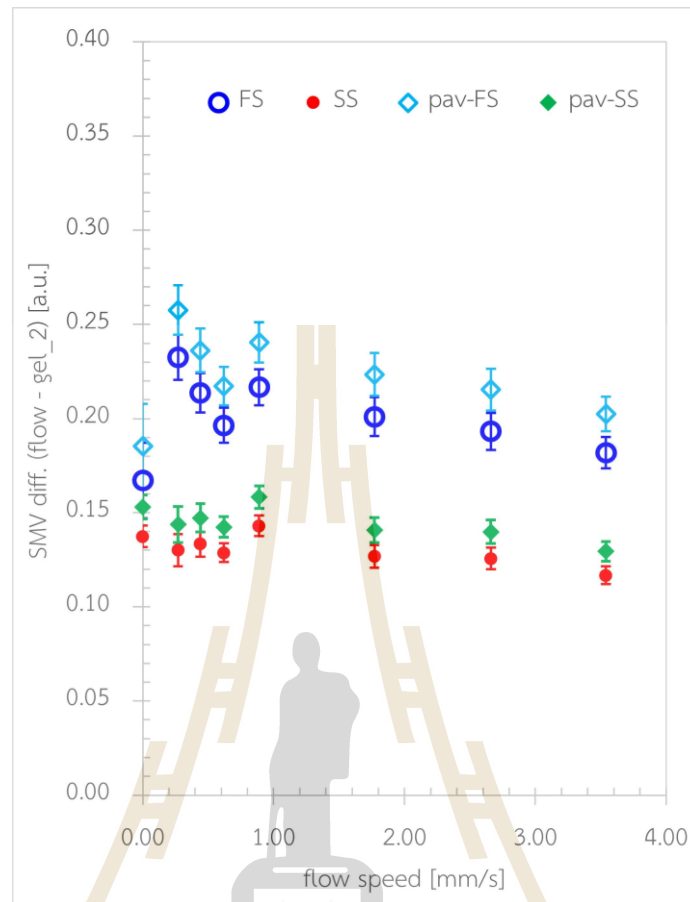


Figure 22 Comparison of angiography value difference (flow – gel_2) in 3 regions at varied flow-speed. (a) SV, (b) SMV, (c) AD.



(b)

Figure 22 Comparison of angiography value difference (flow – gel₂) in 3 regions at varied flow-speed. (a) SV, (b) SMV, (c) AD, (Continued).

มหาวิทยาลัยเทคโนโลยีสุรนารี

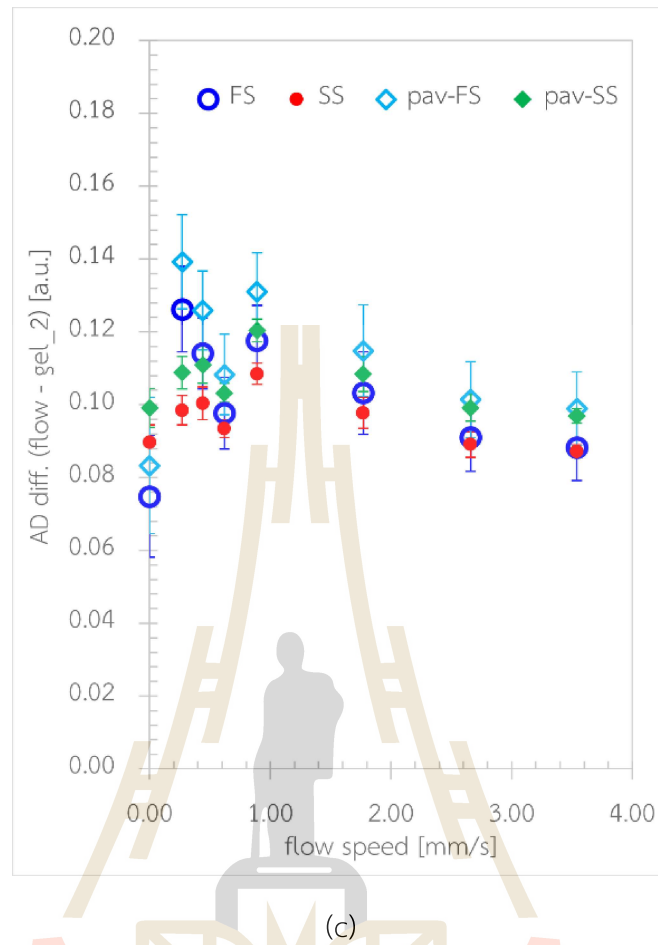


Figure 22 Comparison of angiography value difference (flow – gel_2) in 3 regions at varied flow-speed. (a) SV, (b) SMV, (c) AD, (Continued).

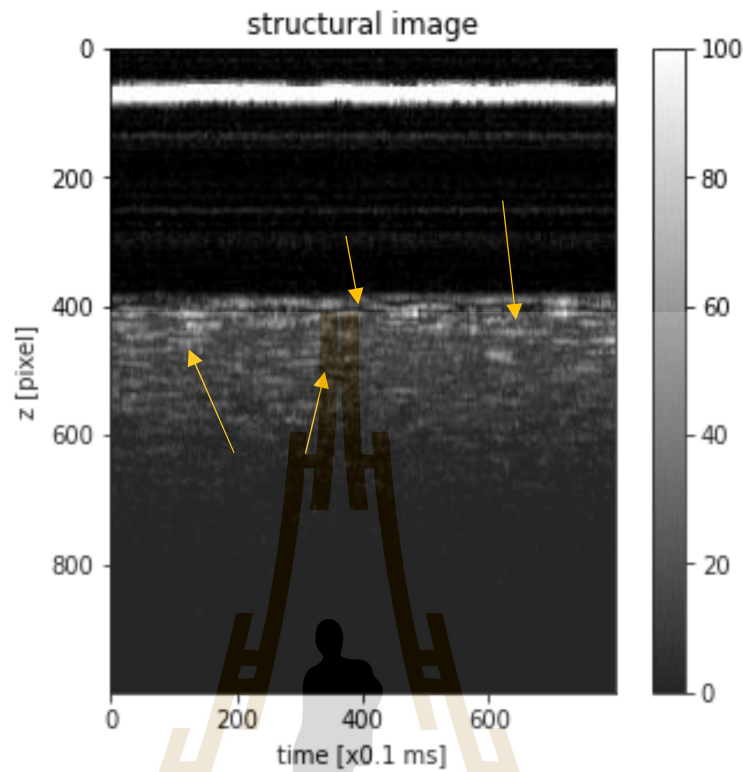


Figure 23 Image of a no-flow BMF inside a capillary at single lateral position (x).

4.3 Performance comparison

It was found that the angiography value is independent on the speed of flow when the data was collected with interframe scan time of 120 ms. Furthermore, even though the intensities should be the same at different flow speeds, they vary slightly. Figure 24 shows that the intensity **CNR** of flow data and static data is -18, ideally it must be zero. In addition, different flow speed data sets, especially slow flow data sets, indicate an inequality of intensity **CNR**. To achieve a reasonable comparison, the inequality must be eliminated. By adding subtraction of the intensity **CNR** (CNR_0) to equation (17) as relative **CNR** (**rel-CNR**) equation (18) (W. Kampong, 2023):

$$\text{rel-CNR} = \text{CNR} - \text{CNR}_0. \quad (18)$$

Then, the performance in terms of **rel-CNR** shows as figure 25. As the results, SMV was provided highest performance when making a comparison with no auxiliary methods.

To achieve higher performance, the auxiliary methods have applied to the SMV algorithm. No auxiliary (FS), SS, pa applied to SMV (pa-FS), and pa-SS methods were analyzed and compared as figure 26. The SS method provide outstanding improvement performance while pa method provides no significant improvement.

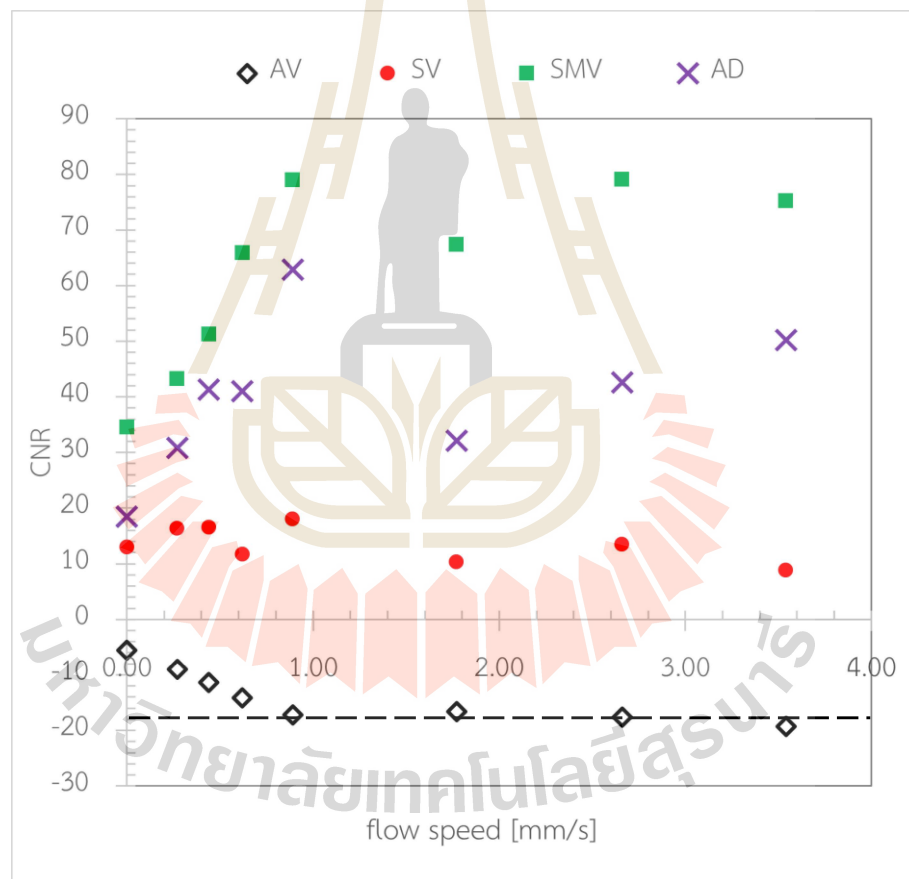


Figure 24 Performance comparison in term of CNR .

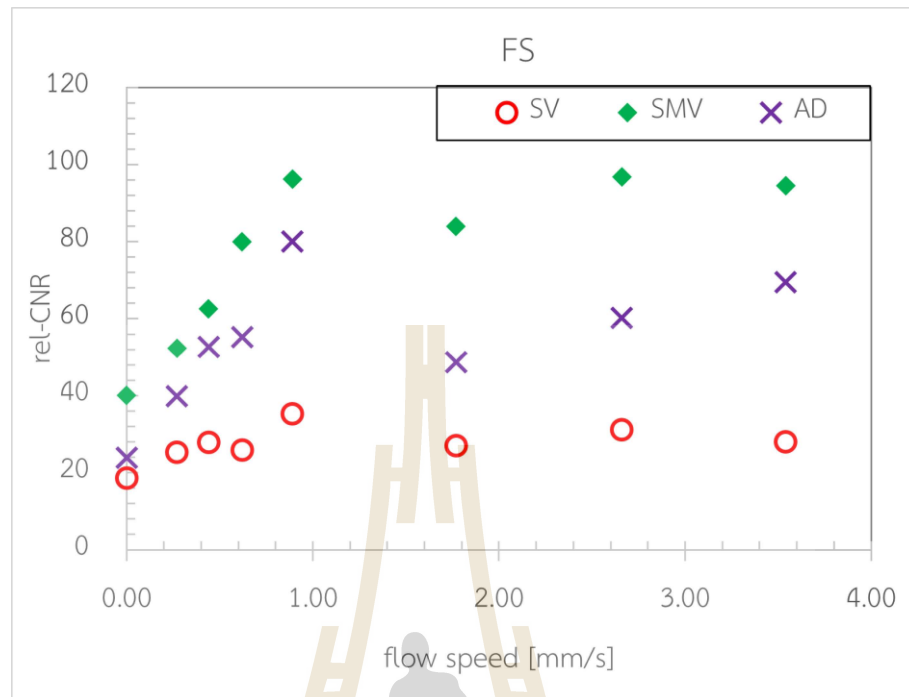


Figure 25 Performance comparison in term of rel-CNR .

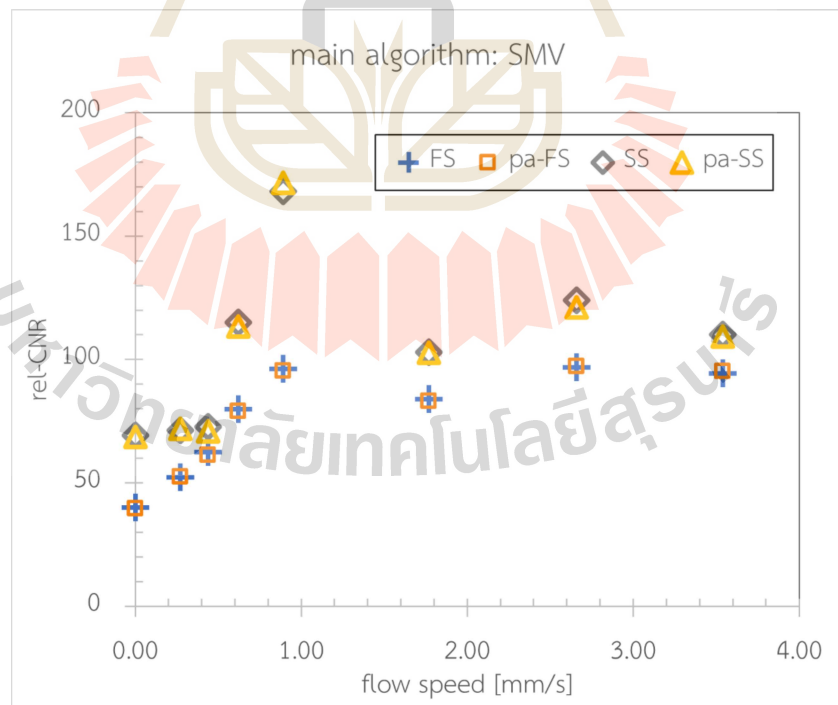


Figure 26 Performance comparison in term of rel-CNR .

To obtain stronger comparison, quantitative improvement was processed. The performance of SV with no auxiliary method (FS-SV) was used as reference. The improvement of OCTA algorithms shown as figure 27. SS-SMV provided the highest improvement of 281%.

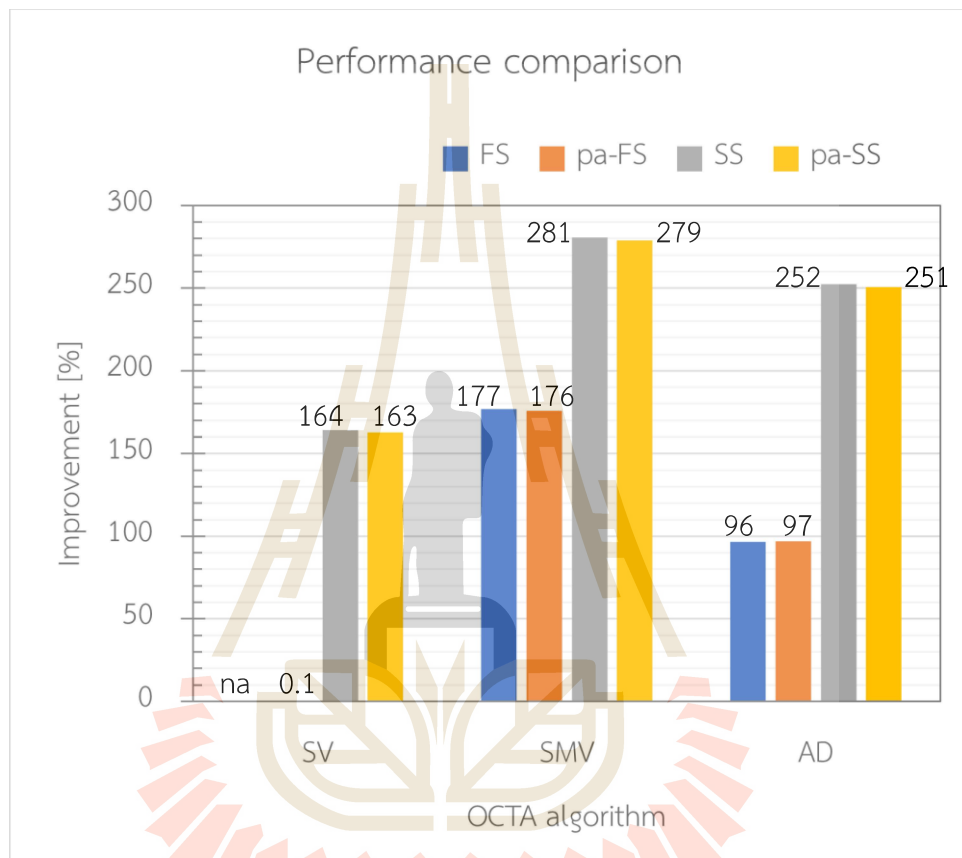


Figure 27 OCTA algorithm performance comparison.

CHAPTER V

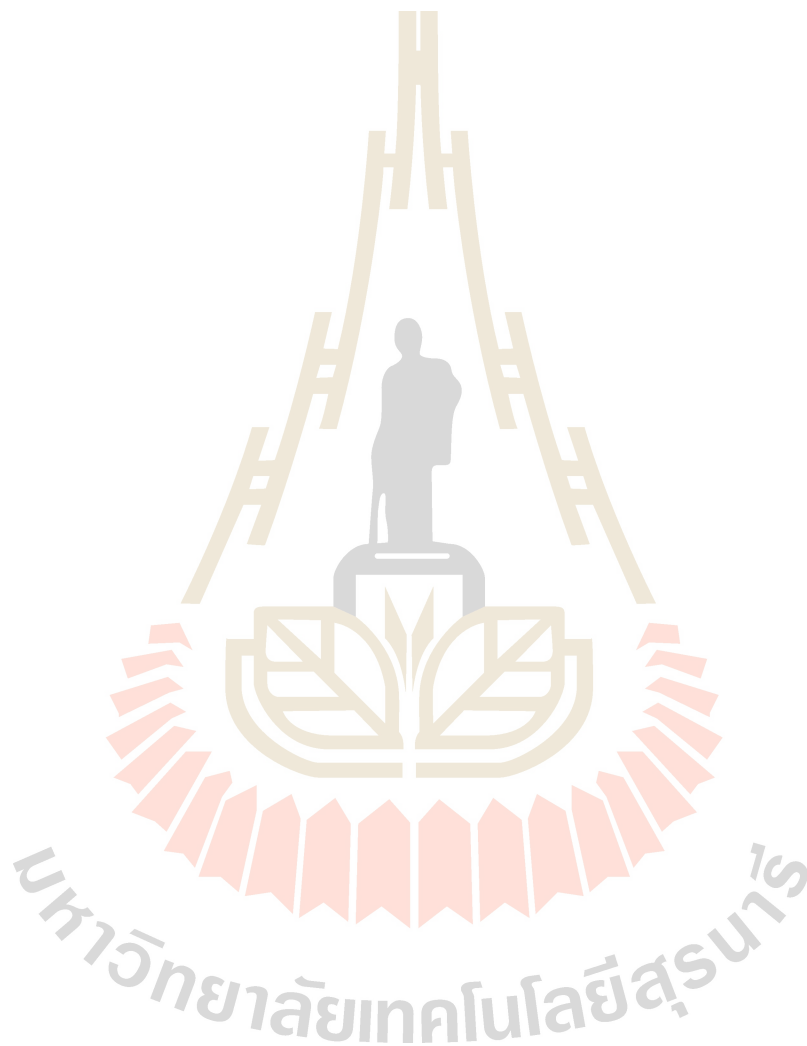
CONCLUSION AND FUTRUE WORK

The OCTA algorithm includes speckle variance (SV), amplitude decorrelation (AD), and speckle-to-mean variance (SMV) and auxiliary techniques of split-spectrum (SS) and pixel-averaging (pa) techniques that were implemented on a custom-developed spectrometer-based SD-OCT imaging system. As illustrated by figure 21 – 22, which indicates that the angiography values are more than the static threshold. Thus, all the algorithms can differentiate flow from static tissues. However, uncontrollable intensity fluctuations necessitated the usage of rel-CNR to suppress non-ideal and inequality intensity data. The experimental results shows that the SMV algorithm provided the highest rel-CNR. Then, the auxiliary method was applied to the SMV algorithm. The result shown that SS method outstanding increases the performance. To quantitative compare, the SV's performance was used as a reference. SS-SMV provide the highest improvement of 281% higher than the reference.

To further study, the number of split-spectrum (M) must be studied to optimize for the OCT system. However, increasing M will be required the computer memory in multiple. Another interesting parameter is Gaussian filters' position. This study's model is that to set the combination of splitting filter be flat-top curve. Another model can be study and compared to optimize the performance.

Although this implemented OCTA imaging system can differentiate flow out of static tissue, it cannot absolutely differentiate high flow and no-flow. Decrease interframe-scan time might be able to track more particle of Brownian motion of no-flow that reduces the randomness of scatterer in no-flow. The flow will then show higher variation from no-flow.

To further optimize the SS-SMV for nailfold microvasculature imaging, the resolution of the image must be considered. The capillary of nailfold microvasculature pattern which used in study and record the pattern change is size 4 microns. Therefore, the resolution of OCTA image provide by the system should be smaller than 3 microns. That size will be able to classify and identify the capillary loop shape.



REFERENCES

มหาวิทยาลัยเทคโนโลยีสุรนารี

REFERENCES

- An, L., Subhush, H., Wilson, D., and Wang, R. (2010). High-resolution wide-field imaging of retinal and choroidal blood perfusion with optical microangiography. *Journal of Biomedical Optics*, 15(2), 026011.
- Ang, M., Tan, A., Cheung, C. M. G., Keane, P., Dolz-Marco, R., Sng, C., and Schmetterer, L. (2018). Optical coherence tomography angiography: a review of current and future clinical applications. *Graefe's Archive for Clinical and Experimental Ophthalmology*, 256. doi:10.1007/s00417-017-3896-2.
- Chen, C.-L., and Wang, R. K. (2017). Optical coherence tomography based angiography [Invited]. *Biomedical Optics Express*, 8(2), 1056-1082. doi:10.1364/BOE.8.001056.
- Chen, C., Shi, W., and Gao, W. (2015). Imaginary part-based correlation mapping optical coherence tomography for imaging of blood vessels in vivo. *Journal of Biomedical Optics*, 20(11), 116009.
- Cutolo, M., Sulli, A., Secchi, M. E., Paolino, S., and Pizzorni, C. (2006). Nailfold capillaroscopy is useful for the diagnosis and follow-up of autoimmune rheumatic diseases. A future tool for the analysis of microvascular heart involvement? *Rheumatology (Oxford)*. 2006 Oct;45 Suppl 4:iv43-6. doi: 10.1093/rheumatology/kel310. PMID: 16980724.
- De Carlo, T. E., Romano, A., Waheed, N. K., and Duker, J. S. (2015). A review of optical coherence tomography angiography (OCTA). *International Journal of Retina and Vitreous*, 1(1), 5. doi:10.1186/s40942-015-0005-8.
- Fingler, J., Schwartz, D., Yang, C., and Fraser, S. E. (2007). Mobility and transverse flow visualization using phase variance contrast with spectral domain optical coherence tomography. *Optics express*, 15(20), 12636-12653. doi:10.1364/OE.15.012636.

- Gao, S. S., Liu, G., Huang, D., and Jia, Y. (2015). Optimization of the split-spectrum amplitude-decorrelation angiography algorithm on a spectral optical coherence tomography system. *Optics Letters*, 40(10), 2305-2308. doi:10.1364/OL.40.002305.
- Gorczyńska, I., Migacz, J. V., Zawadzki, R. J., Capps, A. G., and Werner, J. S. (2016). Comparison of amplitude-decorrelation, speckle-variance and phase-variance OCT angiography methods for imaging the human retina and choroid. *Biomedical Optics Express*, 7(3), 911-942. doi:10.1364/BOE.7.000911.
- Jia, Y., Tan, O., Tokayer, J., Potsaid, B., Wang, Y., Liu, J. J., Huang, D. (2012). Split-spectrum amplitude-decorrelation angiography with optical coherence tomography. *Optics express*, 20(4), 4710-4725. doi:10.1364/OE.20.004710.
- Jonathan, E., Enfield, J., and Leahy, M. J. (2011). Correlation mapping method for generating microcirculation morphology from optical coherence tomography (OCT) intensity images. *Journal of Biophotonics*, 4(9), 583-587. doi:10.1002/jbio.201000103.
- Kim, D. Y., Fingler, J., Werner, J. S., Schwartz, D. M., Fraser, S. E., and Zawadzki, R. J. (2011). In vivo volumetric imaging of human retinal circulation with phase-variance optical coherence tomography. *Biomedical Optics Express*, 2(6), 1504-1513. doi:10.1364/BOE.2.001504.
- Leitgeb, R. A., Werkmeister, R. M., Blatter, C., and Schmetterer, L. (2014). Doppler Optical Coherence Tomography. *Progress in Retinal and Eye Research*, 41, 26-43. doi:https://doi.org/10.1016/j.preteyeres.2014.03.004.
- Lihong V. Wang, H.-i. W. (2007). Optical Coherence Tomography. In *Biomedical Optics* (pp. 181-218): John Wiley and Sons, Inc.
- Liu, G., Jia, Y., Pechauer, A. D., Chandwani, R., and Huang, D. (2016). Split-spectrum phase-gradient optical coherence tomography angiography. *Biomedical Optics Express*, 7(8), 2943-2954. doi:10.1364/BOE.7.002943.

- Mahmud, M., Cadotte, D., Vuong, B., Sun, C., Luk, T., Mariampillai, A., and Yang, V. X. (2013). Review of speckle and phase variance optical coherence tomography to visualize microvascular networks. *Journal of Biomedical Optics*, 18(5), 050901.
- Mariampillai, A., Standish, B. A., Moriyama, E. H., Khurana, M., Munce, N. R., Leung, M. K. K., Yang, V. X. D. (2008). Speckle variance detection of microvasculature using swept-source optical coherence tomography. *Optics Letters*, 33(13), 1530-1532. doi:10.1364/OL.33.001530.
- Sadda, S. R. (2017). Defining the Role of OCT Angiography in Clinical Practice. *Ophthalmology Retina*, 1(4), 261-262. doi:10.1016/j.oret.2017.05.001
- Shahipasand, S., Mohammed-Noriega, J., Sim, D., Gizzi, C., & Kortum, K. (2019). Nailfold capillaroscopy with a commercially available optical coherence tomography angiography for ophthalmic use. *Adv Ophthalmol Vis Syst*, 9(2), 38-42.
- Spaide, R. F., Fujimoto, J. G., Waheed, N. K., Sadda, S. R., and Staurengi, G. (2018). Optical coherence tomography angiography. *Progress in Retinal and Eye Research*, 64, 1-55. doi:https://doi.org/10.1016/j.preteyeres.2017.11.003.
- Wang, L. V., and Wu, H. I. (2012). *Biomedical optics: principles and imaging*. John Wiley and Sons.
- Wang, R. K. (2010). Optical Microangiography: A Label-Free 3-D Imaging Technology to Visualize and Quantify Blood Circulations Within Tissue Beds In Vivo. *IEEE Journal of Selected Topics in Quantum Electronics*, 16(3), 545-554. doi:10.1109/JSTQE.2009.2033609.
- Wang, R. K., Jacques, S. L., Ma, Z., Hurst, S., Hanson, S. R., and Gruber, A. (2007). Three dimensional optical angiography. *Optics express*, 15(7), 4083-4097. doi:10.1364/OE.15.004083.
- Winkelmann, J. A., Eid, A., Spicer, G., Almassalha, L. M., Nguyen, T.-Q., and Backman, V. (2019). Spectral contrast optical coherence tomography angiography enables single-scan vessel imaging. *Light: Science and Applications*, 8(1), 7. doi:10.1038/s41377-018-0117-7.

- Wojtkowski, M., Srinivasan, V. J., Ko, T. H., Fujimoto, J. G., Kowalczyk, A., and Duker, J. S. (2004). Ultrahigh-resolution, high-speed, Fourier domain optical coherence tomography and methods for dispersion compensation. *Optics express*, 12(11), 2404-2422.
- Yousefi, S., Zhi, Z., and Wang, R. K. (2011). Eigendecomposition-based clutter filtering technique for optical micro-angiography. *IEEE transactions on biomedical engineering*, 58(8), 10.1109/TBME.2011.2152839. doi:10.1109/TBME.2011.2152839.
- Yu, L., and Chen, Z. (2010). Doppler variance imaging for three-dimensional retina and choroid angiography. *Journal of Biomedical Optics*, 15(1), 016029.
- Mahnaz Etehad Tavakol et al., (2015). Nailfold Capillaroscopy in Rheumatic Diseases: Which Parameters Should Be Evaluated? *BioMed Research International*. Volume 2015, Article ID 974530, 17 pages. <http://dx.doi.org/10.1155/2015/974530>.
- Darryn Rennie (2015). Nailfold dermatoscopy in general practice. *Australian Journal for General Practitioners*. Volume 44.
- Pongchaidecha, M., and Muangkaew, R. (2015). Evaluation of Nail-fold Capillary Structures (Diameter and Tortuosity) in Carbamazepine-Treated Patients. *Thai J Pharmacol*; Vol, 37(1), 17.
- Rolland, J. P., Meemon, P., Murali, S., Thompson, K. P., and Lee, K. S. (2010). Gabor based fusion technique for optical coherence microscopy. *Optics express*, 18(4), 3632-3642.
- Meemon, P., Lenaphet, Y., and Widjaja, J. (2021). Spectral fusing Gabor domain optical coherence microscopy based on FPGA processing. *Applied Optics*, 60(7), 2069-2076.
- Meemon, P., Palawong, K., and Pongchalee, P. (2014, March). Simplified methods of design, implementation, and characterization of a spectrometer-based FD-OCT. In *Three-Dimensional and Multidimensional Microscopy: Image Acquisition and Processing XXI* (Vol. 8949, pp. 232-237). SPIE.

Thanomsit, C., Saetiew, J., and Meemon, P. (2022). Optical coherence tomography as an alternative tool for evaluating the effects of glyphosate on hybrid catfish (*Clarias gariepinus* × *Clarias macrocephalus*). *Toxicology Reports*, 9, 181-190.

Saetiew, J. (2018). Development of optical tomography technique for monitoring biofilm formation (Doctoral dissertation, School of Physics Institute of Science Suranaree University of Technology).



CURRICULUM VITAE

Name	Wuttikorn Kampong
Date of Birth	3 August 1995
Place of Birth	Khon Kaen, Thailand
Education	Bachelor's degree in Physics (2014 – 2017), Khon Kaen University, Thailand. Bachelor of Science (Physics), (Second class honors), GPA = 3.45/4.00.
Publications	Kampong, W., et al. "Performance comparison of amplitude-decorrelation and speckle variance algorithms in spectrometer-based OCT angiography." <i>Journal of Physics: Conference Series</i> . Vol. 2431. No. 1. IOP Publishing, 2023.
Grants and Fellowships	The Development and Promotion of Science and Technology Talents Project, Suranaree University of Technology, and the National Research Council of Thailand.
Position and Place of Work	Demonstration Secondary School Nakhon Ratchasima Rajabhat University, Thailand.